5455553
33p

Atmospheric and
Environmental Research, Inc.

Momentum and energy assessments with NASA and other model and data assimilation systems

Annual report for project NAS5-98179
(AER project P785)
Option I period

David Salstein
Peter Nelson
Wenjie Hu

Atmospheric and Environmental Research, Inc
131 Hartwell Avenue
Cambridge, MA 02139

(salstein@aer.com)

Annual report for Option I

During the period funded under Option I of the subject contract, we have been involved in several aspects of the research under support of the NASA Global Modeling and Analysis Program. They can be outlined as follows:

1. Study of aspects of dynamics of torques and angular momentum based on the Goddard GEOS and other analyses. We also have examined regions where rapid changes in the angular momentum from mass shifts have yielded large variability in momentum. Figures illustrating these points are given in Attachment 1.

2. Study of the how models participating in the second Atmospheric Model Intercomparison Project (AMIP-2) have success in simulating certain large-scale quantities. Besides NASA models, a fair number of others have submitted results to the archives of AMIP-2. We have enlarged our first focus on angular momentum of the atmosphere to include large-scale water vapor and vapor fluxes, and other aspects of atmospheric variability. To date, 16 models results are available for this assessment. Some of our results from the AMIP-2 experiment are given as Attachment 2.

3. Study of the energetics and momentum cycle from certain runs from the Goddard Laboratory for Atmospheres (latest simulation: Sud and Walker, 1999), and other models as well. Some results are synthesized in "Diabatic heating and the Atmospheric Energy Cycle," by D. Salstein, to appear in the proceedings of the Jose P. Peixoto Memorial Symposium, University of Lisbon Press, which is given here as Attachment 3. Further work in this topic is being prepared for the chapter on diabatic heating of the revised edition of *Physics of Climate* (originally Peixoto and Oort 1992). We have also assessed such changes in diabatic heating and related energetics in the community climate model (CCM3) of NCAR, especially with a new radiation code developed at AER. One example of the figures is the generation of APE by latent heating, difference between the CCM3 with and without the new radiation code, named RRTM. Techniques for the generation of APE were developed under this NASA project and its predecessors. One such figure, given as an example, is included as Fig. 3a.1, following Attachment 3.

4. Analyzing modes of climate of the atmosphere, especially the Arctic and North Atlantic Oscillations. This topic relates to the interannual variability found in the NASA Goddard Models, GEOS-1 DAS reanalysis, and other reanalyses. The work was done collaboratively with Judah Cohen of AER. The abstract of a recently submitted paper on this topic is given as Attachment 4.

More details will be given in published works and in the Final report of the project.

David Salstein
Principal Investigator

References

Peixoto, J. P. and A. H. Oort, 1992: Physics of Climate, AIP Press, New York.

Sud, Y. C., G. K. Walker, 1999: Microphysics of Clouds with the Relaxed Arakawa–Schubert Scheme (McRAS). Part II: Implementation and Performance in GEOS II GCM. Journal of the Atmospheric Sciences: Vol. 56, No. 18, pp. 3221–3240.

Attachment 1

The angular momentum mass term based on both the NASA GEOS-1 DAS and the NCEP-NCAR reanalyses is given between 1991 and 1995. We focus on the large jump occurring in the middle of 1992 (Fig. 1.1). This jump also appears in the NCEP-NCAR reanalyses. (Fig. 1.2; though for 1991-2000). Noting that this jump in 1992 is also noted in independent measures of the length of day (Fig. 1.3 and 1.4) allows us to presume that it is a real signature. We then analyze the period June- July 1992 to determine that the change in these values are especially strong over the middle to high latitude southern hemisphere. The fractional covariance between belt and global signal is highest near 40 S latitude (Fig. 1.5). Focusing on that we look at 5 day sequences of the anomalies of pressure-based atmospheric angular momentum (Fig. 1.6) to see the rapid changes across the southern oceans near the 40 degree parallel. The movement is even more obvious with the daily progression between July 12 and 17 (Fig. 1.7), at the height of the episode.

Lastly we wish to contrast the two torque mechanisms that convey angular momentum between the atmosphere and solid earth for 1991-2000, here from the NCEP-NCAR analyses. In the mountain torque (Fig. 1.8), normal pressure gradients across topographic features, the high frequencies, such as those associated with the synoptic storms and signals are most evident, whereas the friction torque (Fig. 1.9), a tangential stress caused by low-level winds is much steadier.

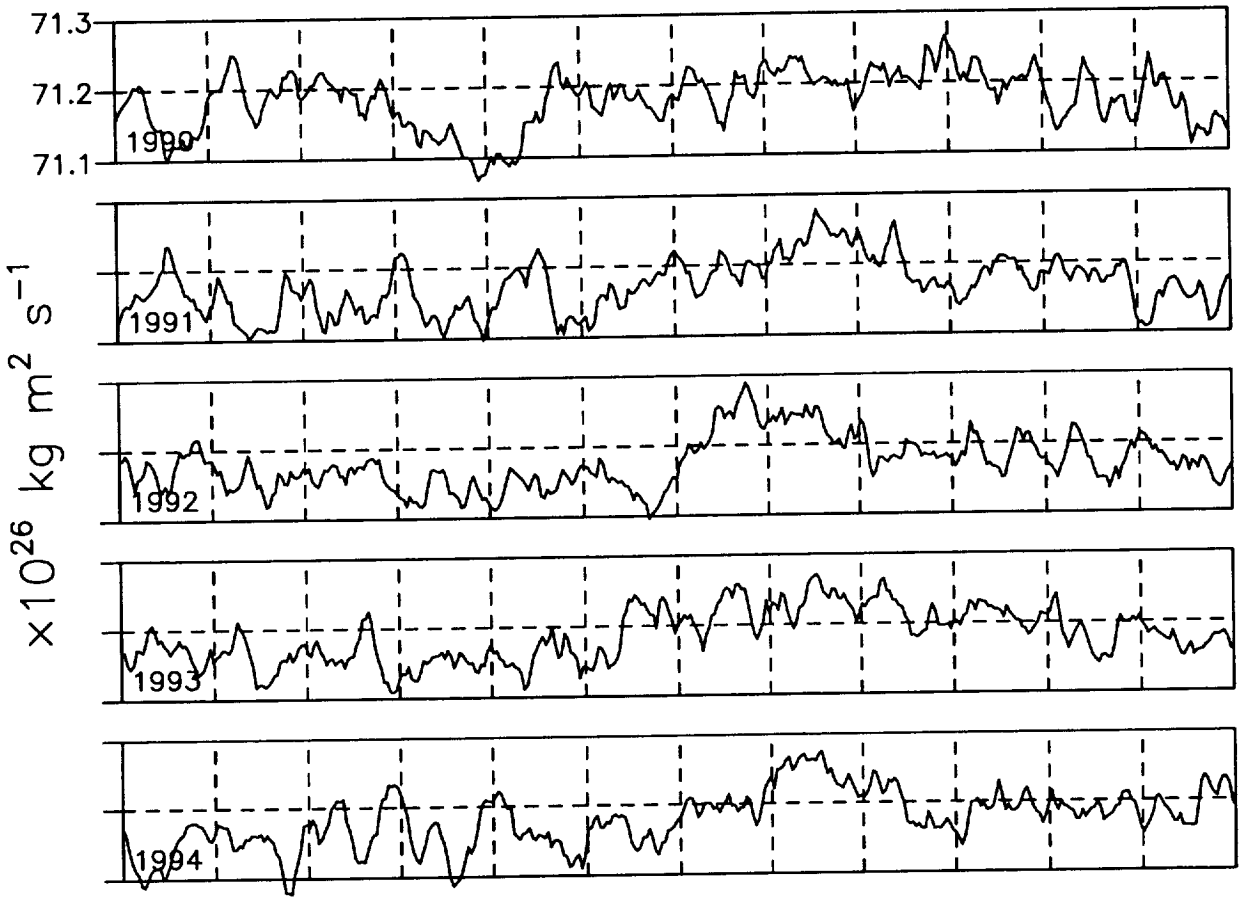
Atmospheric Angular Momentum, Mass Term (M^P)
NASA GEOS–1 DAS
71.3
71.2
71.1
1990
1991
1992
1993
1994
$\times 10^{26}$ kg m^2 s^{-1}

Fig. 1.1

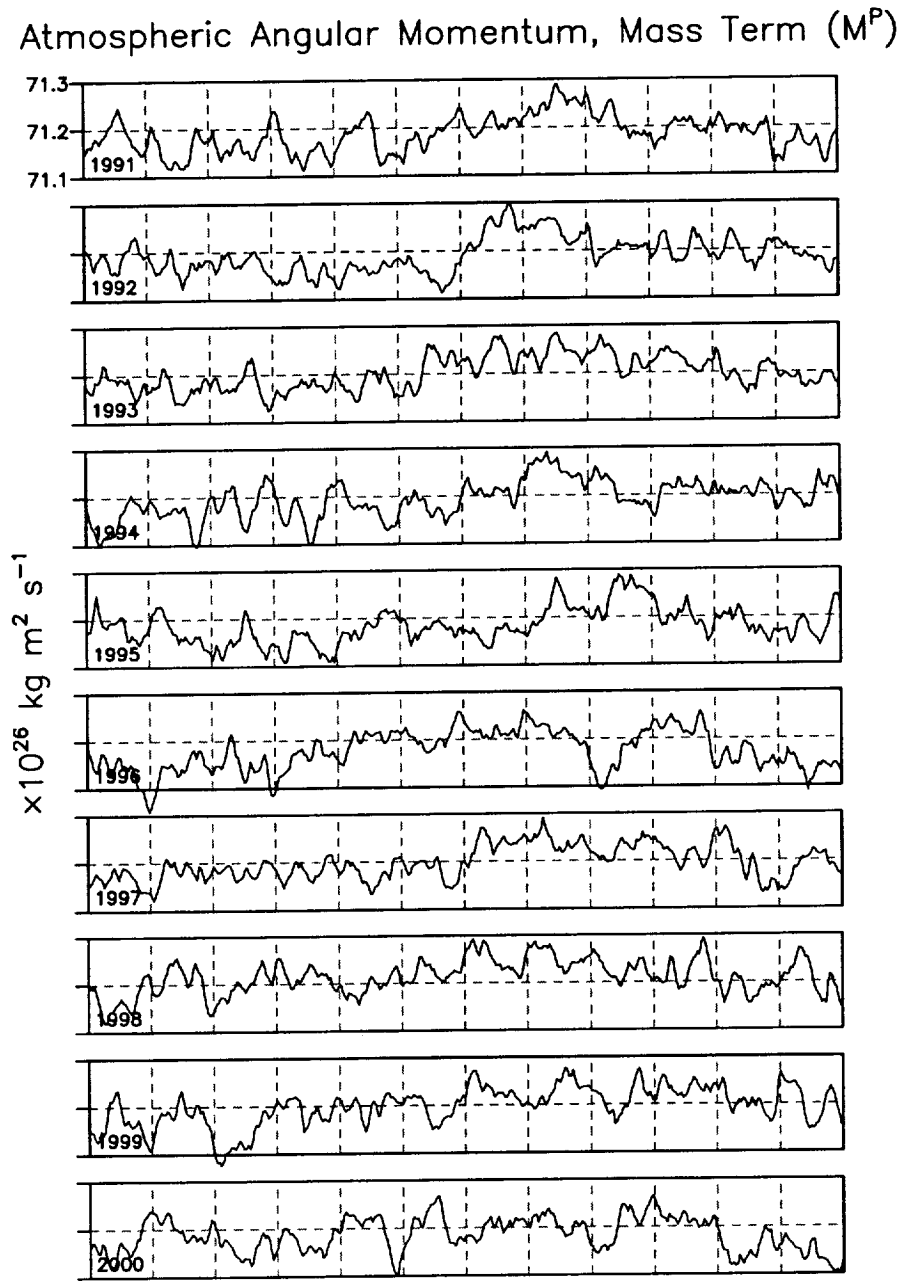
Atmospheric Angular Momentum, Mass Term (M^P)
71.3
71.2
71.1
1991
1992
1993
1994
1995
1996
1997
1998
1999
2000
$\times 10^{26}$ kg m^2 s^{-1}

Fig. 1.2

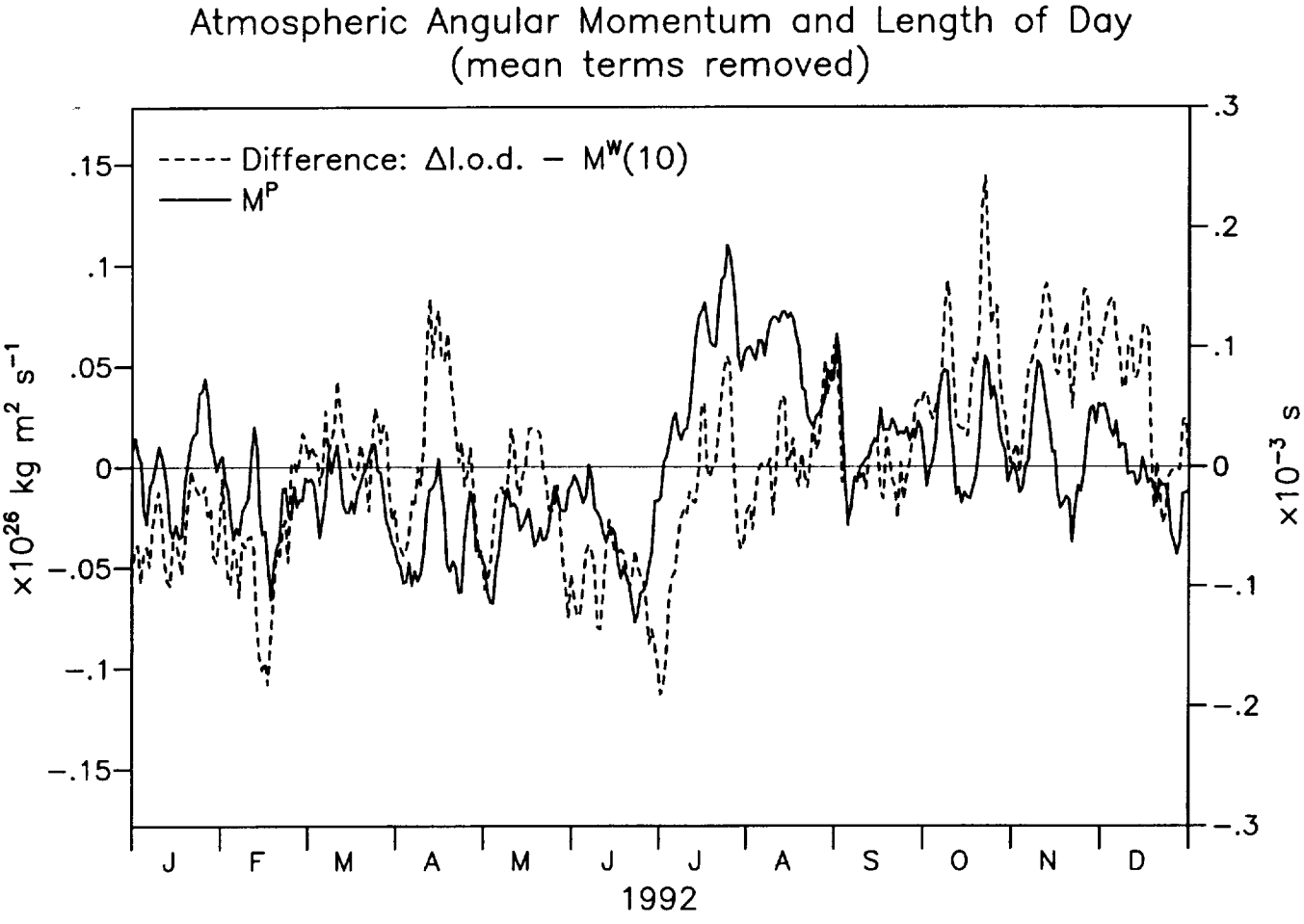
Atmospheric Angular Momentum and Length of Day
(mean terms removed)
----- Difference: ΔI.o.d. − M^W(10)
—— M^P
.15
.1
.05
0
−.05
−.1
−.15
×10^26 kg m^2 s^-1
.3
.2
.1
0
−.1
−.2
−.3
×10^-3 s
J F M A M J J A S O N D
1992

Fig. 1.3

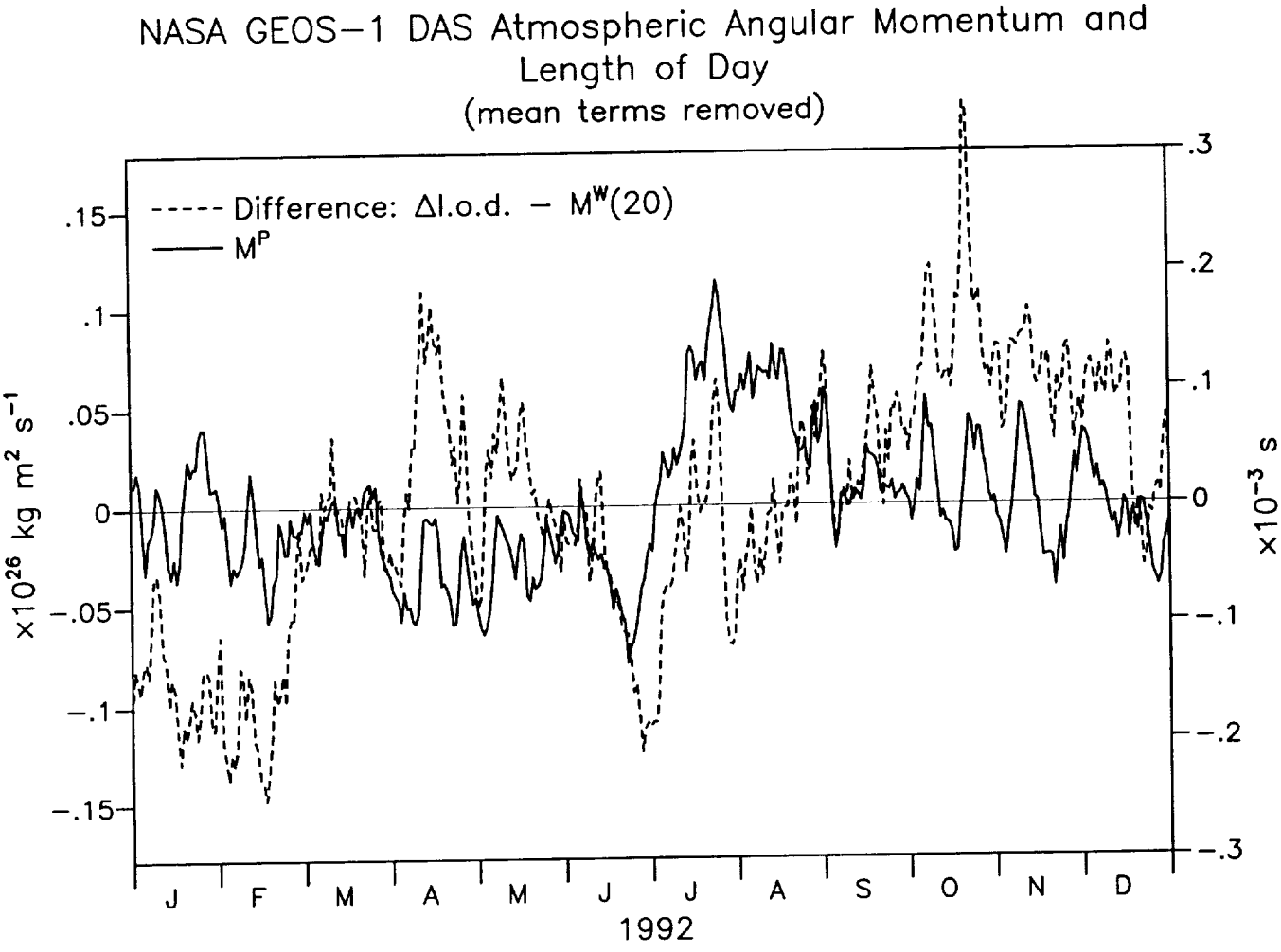
NASA GEOS–1 DAS Atmospheric Angular Momentum and Length of Day
(mean terms removed)
----- Difference: Δl.o.d. – M^W(20)
—— M^P
.15
.1
.05
0
–.05
–.1
–.15
x10^26 kg m^2 s^-1
.3
.2
.1
0
–.1
–.2
–.3
x10^-3 s
J F M A M J J A S O N D
1992

Fig. 1.4

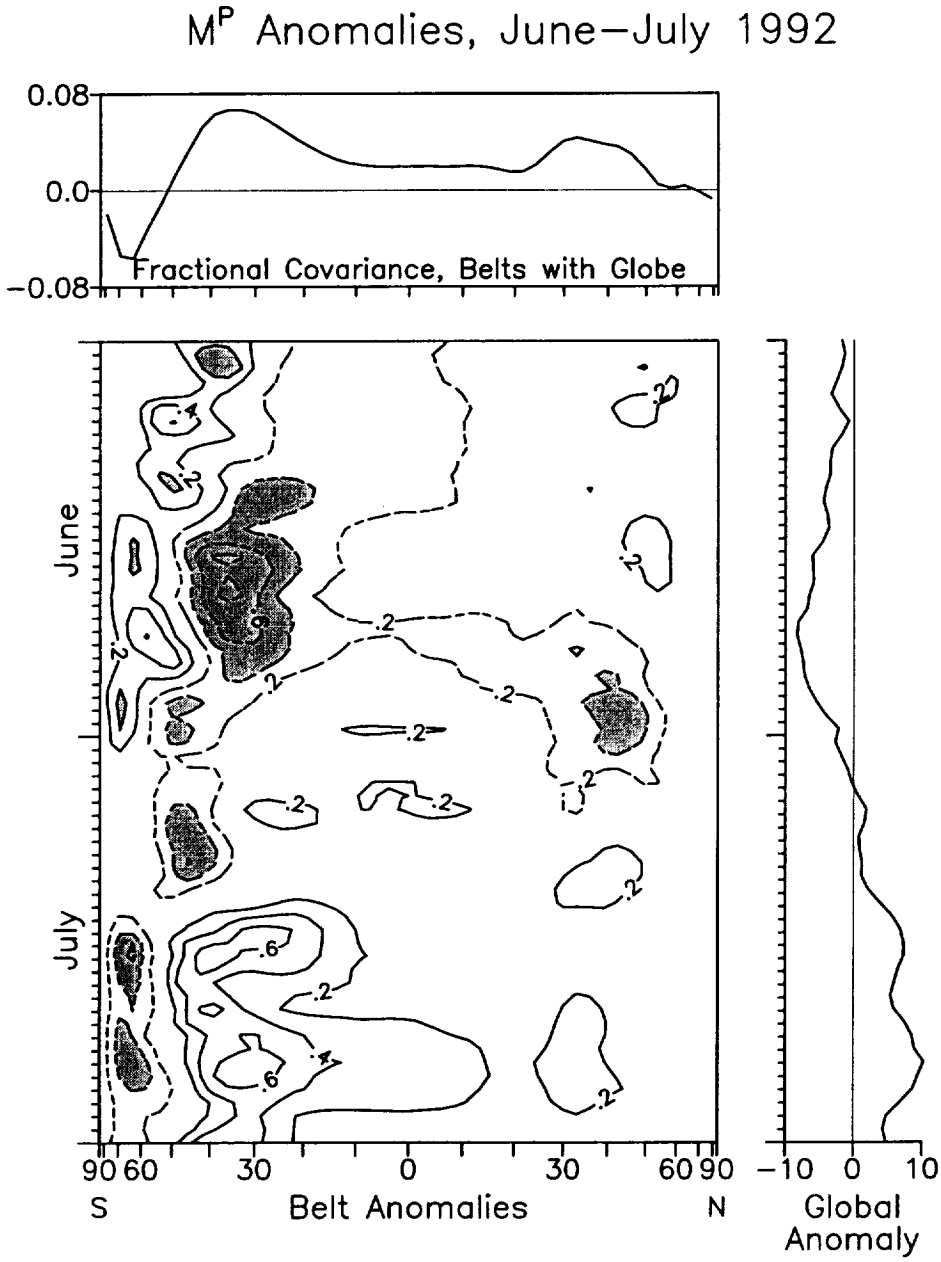
M^P Anomalies, June–July 1992
0.08
0.0
−0.08
Fractional Covariance, Belts with Globe
June
July
90 60 30 0 30 60 90
S
Belt Anomalies
N
−10 0 10
Global Anomaly

Fig. 1.5

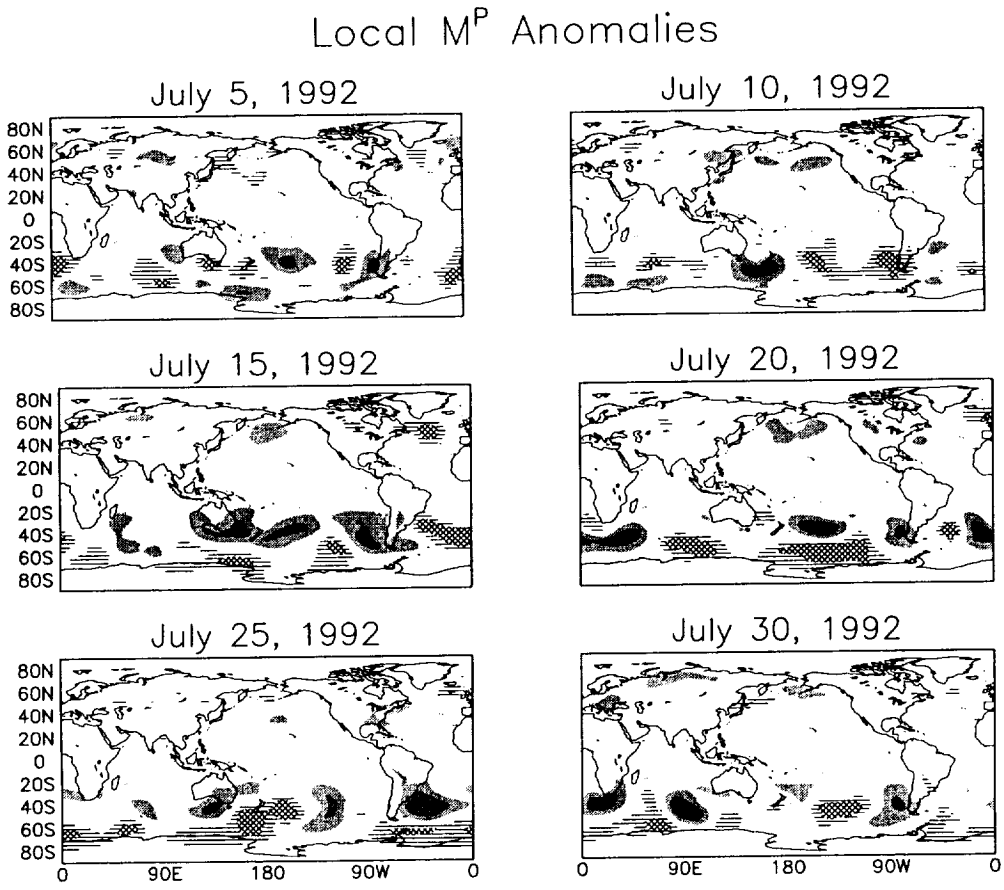
Local M^P Anomalies
July 5, 1992
July 10, 1992
July 15, 1992
July 20, 1992
July 25, 1992
July 30, 1992
80N
60N
40N
20N
0
20S
40S
60S
80S
0
90E
180
90W
0

Fig. 1.6

Local M^P Anomalies

July 12, 1992

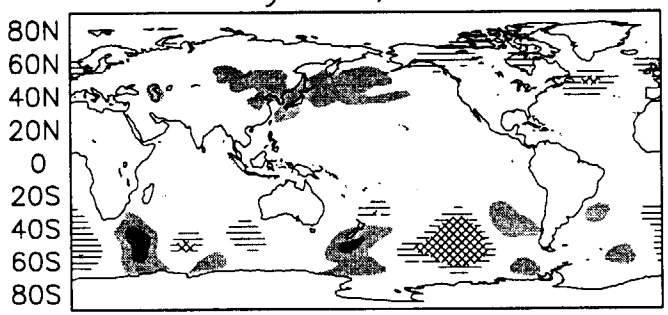

July 13, 1992

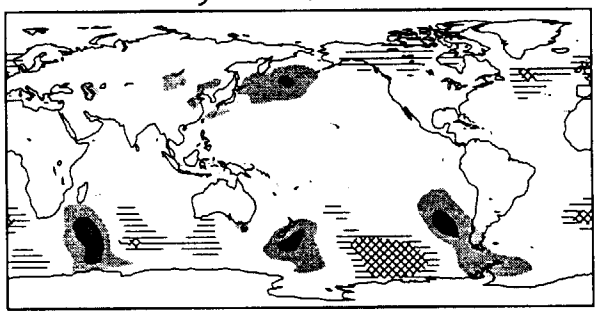

July 14, 1992

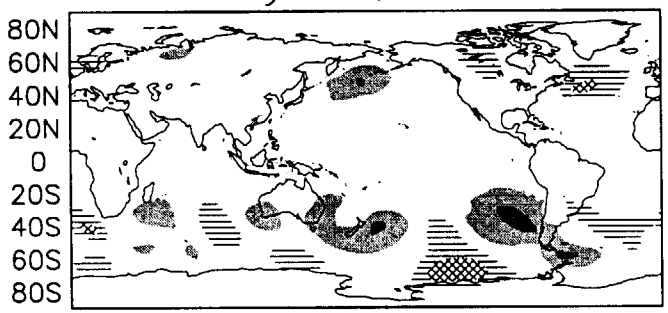

July 15, 1992

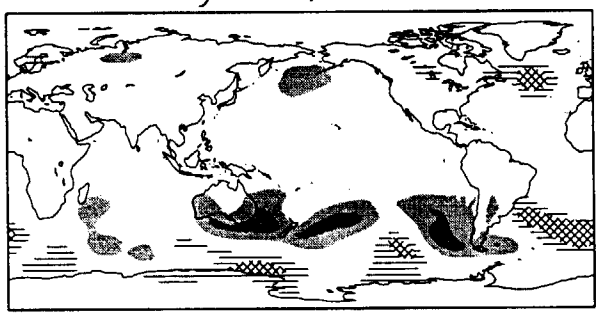

July 16, 1992

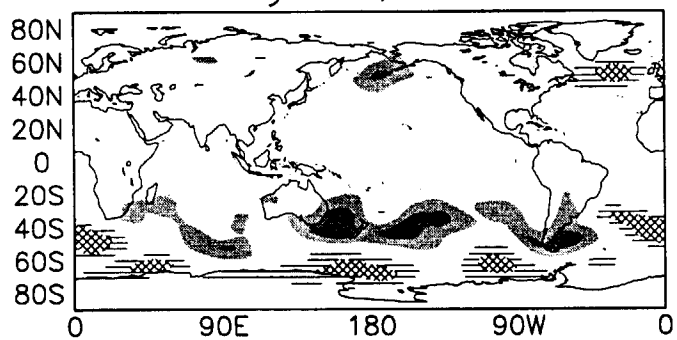

July 17, 1992

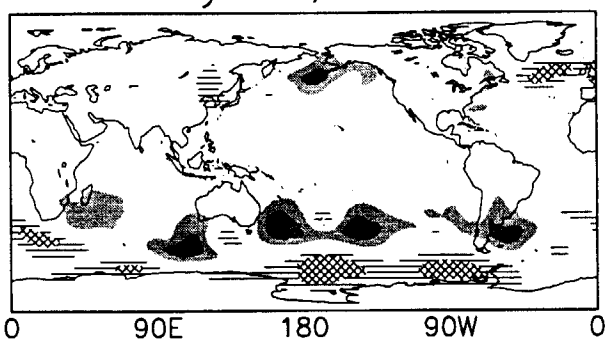

Fig. 1.7

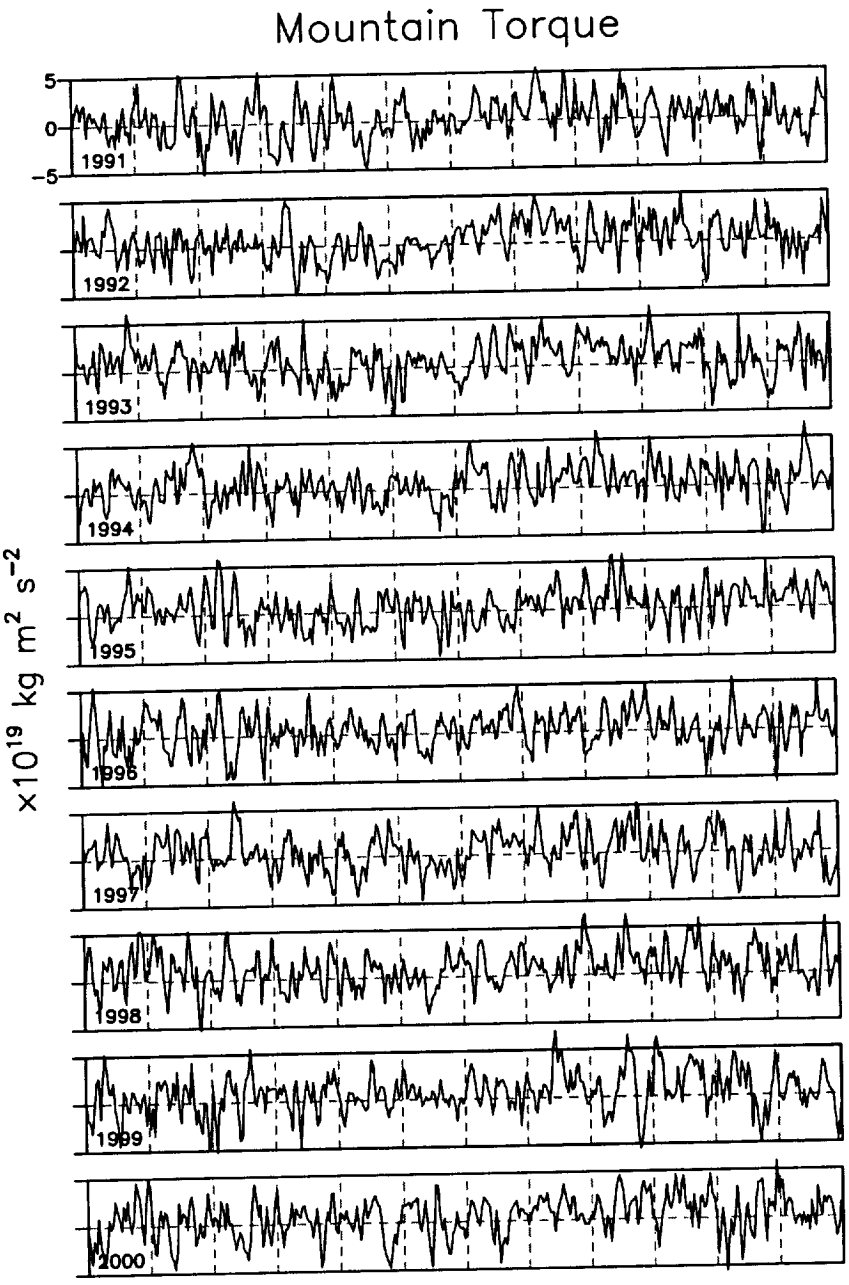
Mountain Torque
5
0
-5
1991
1992
1993
1994
1995
1996
1997
1998
1999
2000
x10^19 kg m^2 s^-2

Fig. 1.8

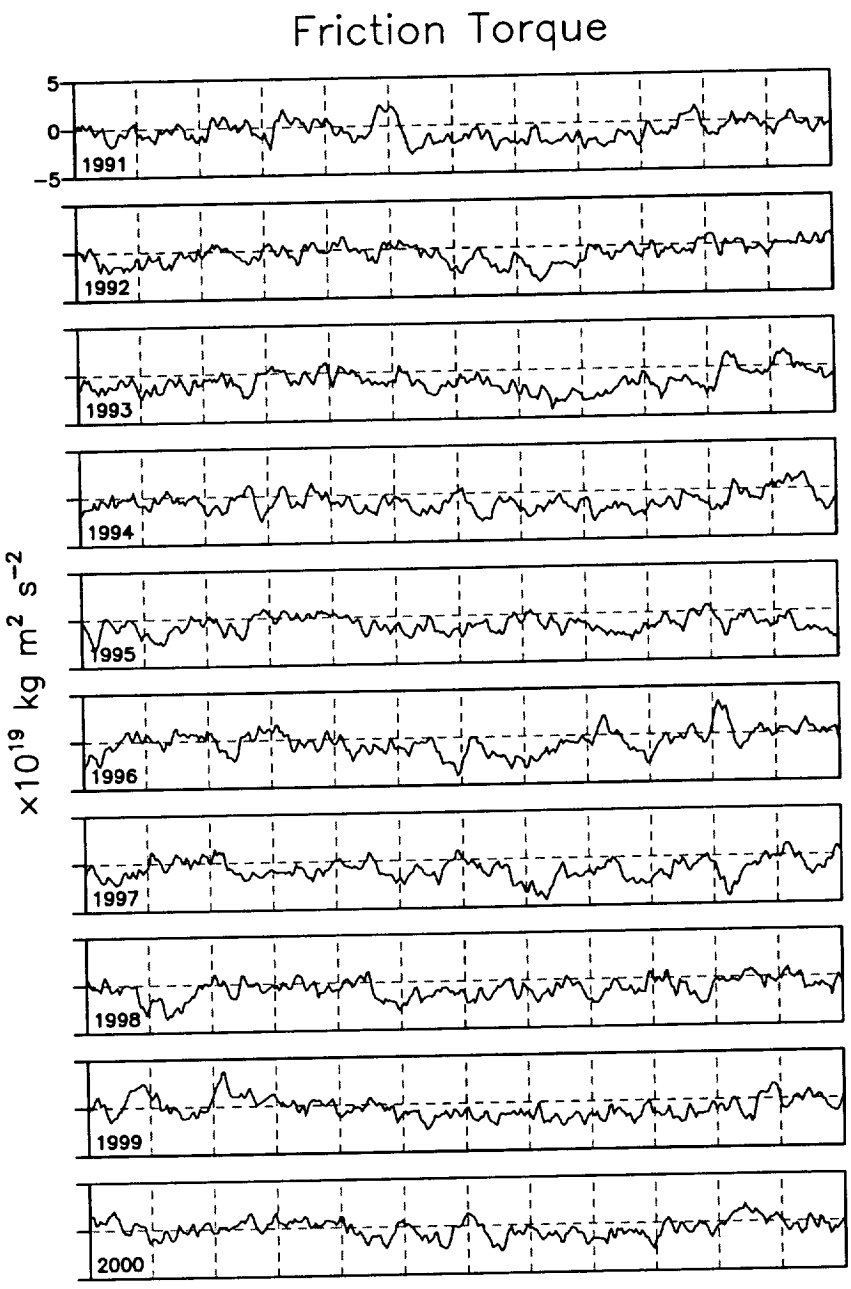
Friction Torque
5
0
−5
1991
1992
1993
1994
1995
1996
1997
1998
1999
2000
x10^19 kg m^2 s^-2

Fig. 1.9

Attachment 2

We have compared several models participating in the Atmospheric Model Intercomparison Project, a project in which the general circulation models in the world's major weather centers have been run with prescribed sea-surface temperatures.. In the prior annual report, we noted that two models were available. We noted that for angular momentum, model-based quantities had improved the simulations, mostly because of improved parameterizations at the lowest latitudes. With sixteen models now available, we focus on the characteristics of the mean, and of the spread amongst models as well. The 17 year mean (1979-1995) of the AMIP-2 experiment has allowed us to examine the angular momentum between different ENSO years, and we have also studied a composite seasonal circulation. The 17-year mean appears to have a new bias of the models in AMIP-2 (Fig. 2.1) but the seasonal and interannual components are reasonably well simulated (Fig. 2.2 and 2.3). We note that eight of the model (four high, including the GLA, and four low) all demonstrate different characteristics in their departure from the NCEP-NCAR reanalyses in the zonal winds, from which are integrated the global atmospheric angular momentum (Figs. 2.4 and 2.5).

We have also looked at the large-scale models for AMIP moisture and moisture fluxes. Here, though we have focused more at the regional balances, because of other considerations, and this work is largely sponsored by other agency. Nevertheless, we were able to look at the flux divergence in the North American region, and see the progression of all the AMIP models. To the suite of AMIP models and that from reanalysis, we compare them with a NASA model, that of Sud and Walker (1999), including the McRAS scheme. That model result, the mean signal for each month of 4 years, is given here (Fig. 2.6) shows the seasonal progression of water divergence across North America. The mean seasonal signature is compared with the suite of AMIP models in Fig. 2.7

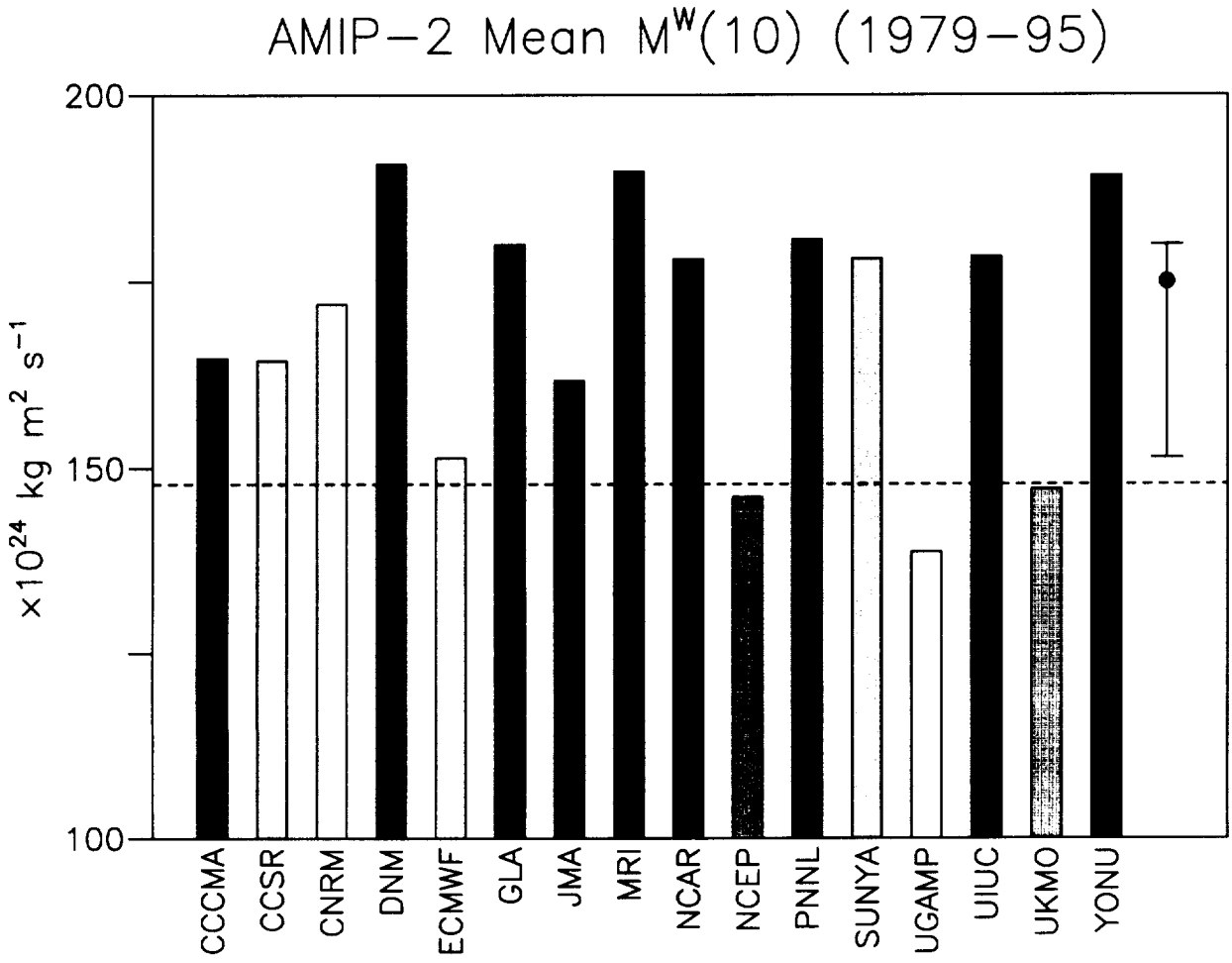
AMIP−2 Mean M^W(10) (1979−95)
200
150
100
x10^24 kg m^2 s^-1
CCCMA
CCSR
CNRM
DNM
ECMWF
GLA
JMA
MRI
NCAR
NCEP
PNNL
SUNYA
UGAMP
UIUC
UKMO
YONU

Fig. 2.1

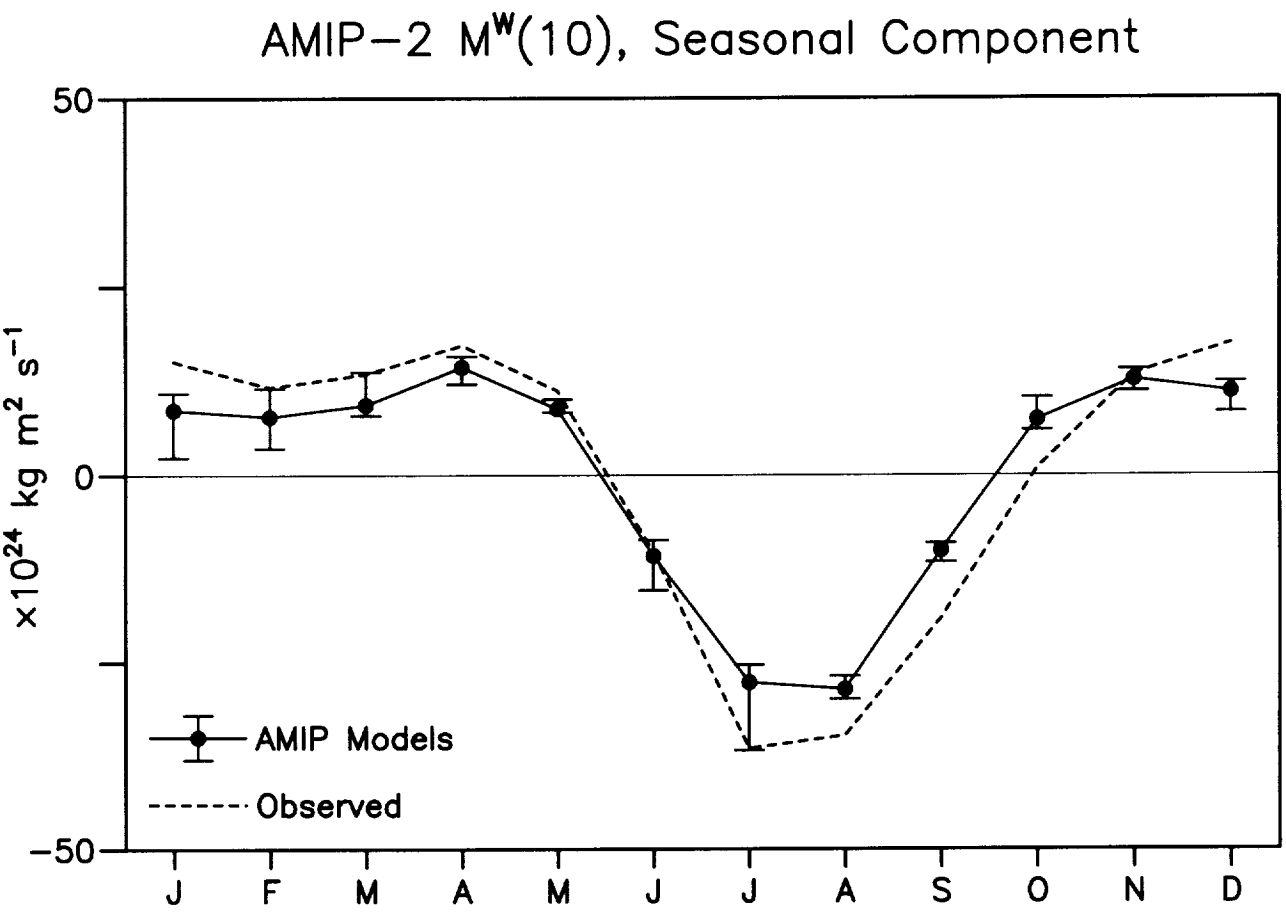
AMIP−2 M^W(10), Seasonal Component
50
0
−50
×10^24 kg m^2 s^−1
AMIP Models
Observed
J
F
M
A
M
J
J
A
S
O
N
D

Fig. 2.2

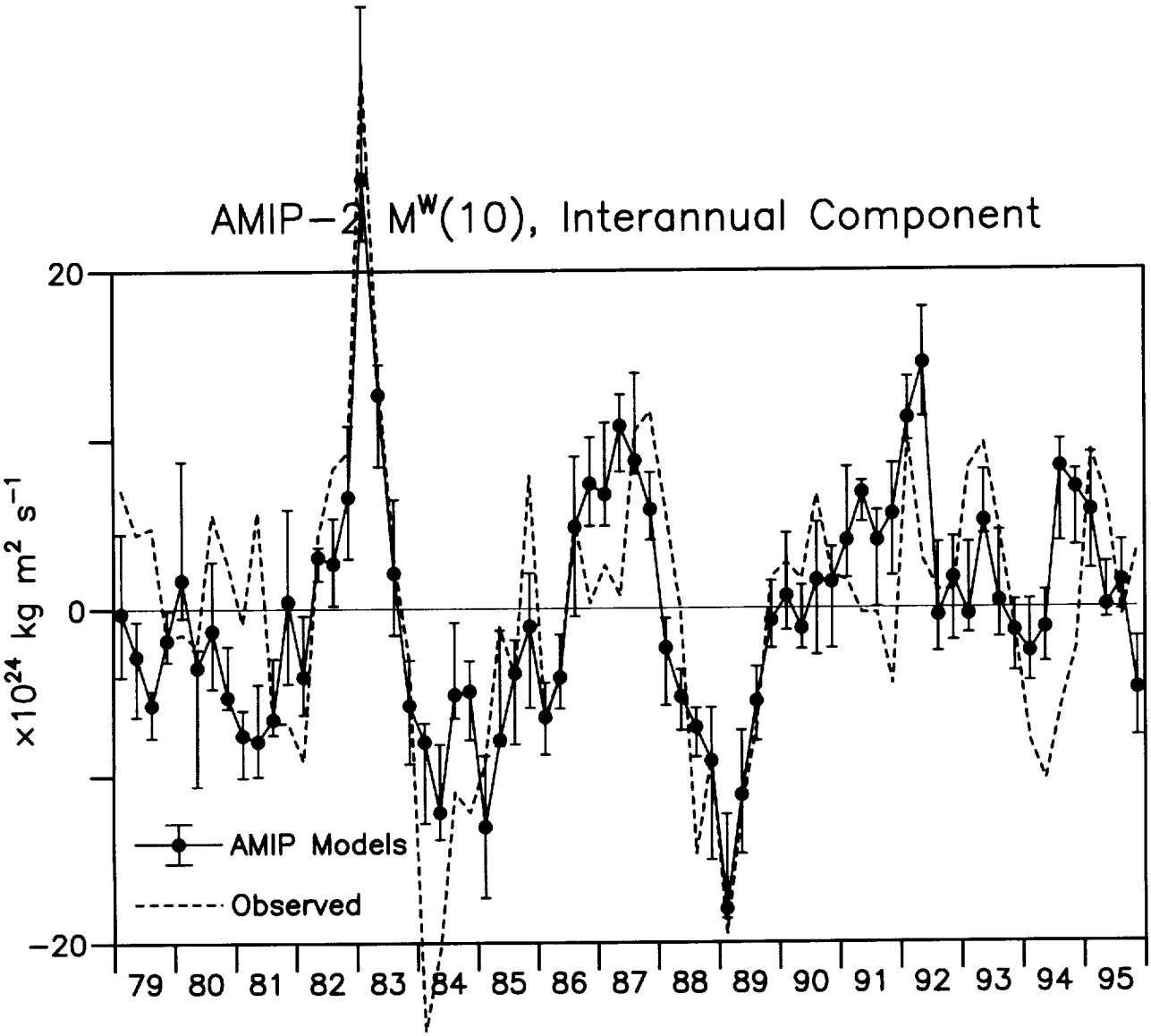
AMIP–2 $M^w(10)$, Interannual Component
20
0
−20
$\times 10^{24}$ kg m^2 s^{-1}
AMIP Models
Observed
79
80
81
82
83
84
85
86
87
88
89
90
91
92
93
94
95

Fig. 2.3

AMIP−2 [u], 1979−1995

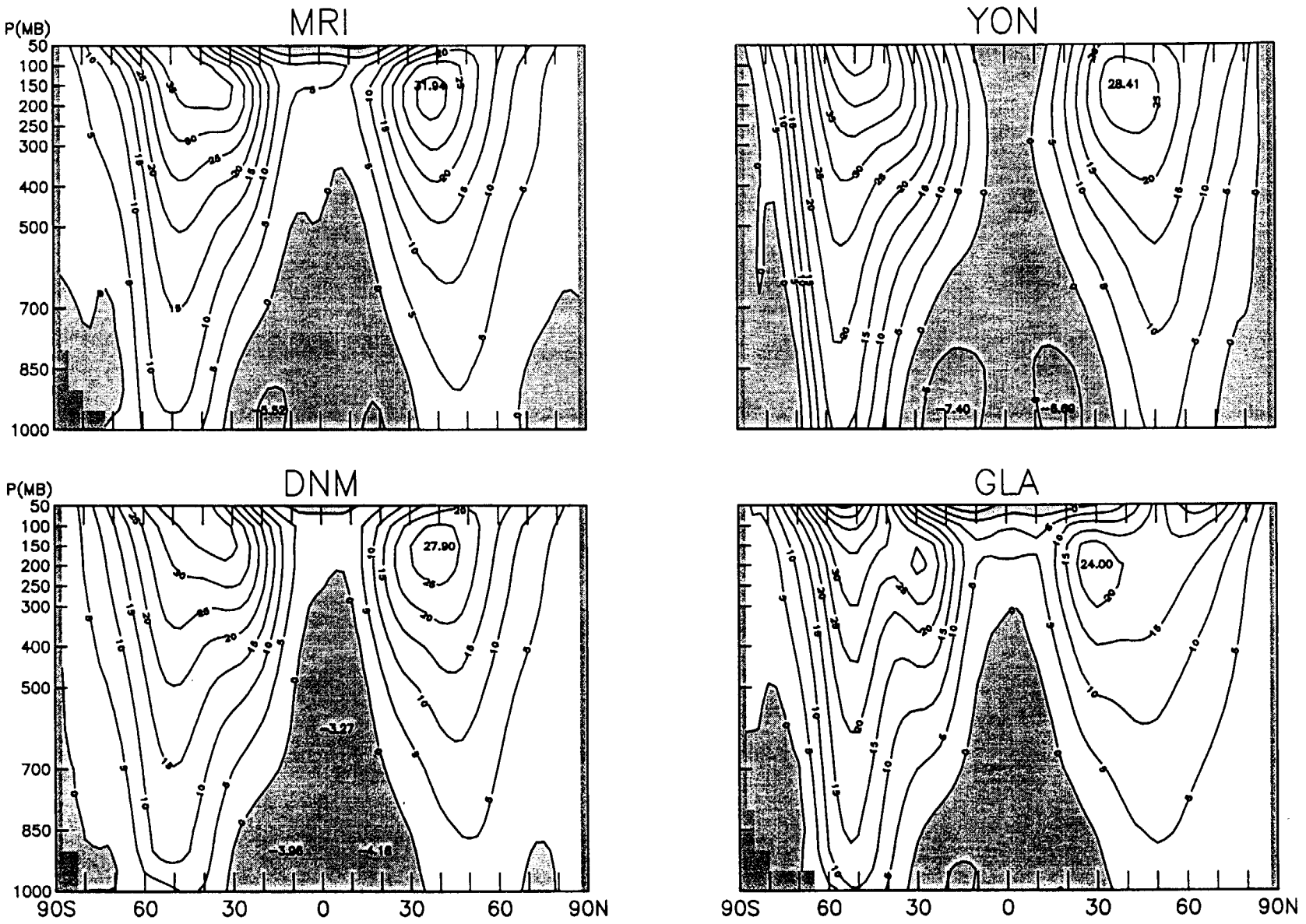

Fig. 2.4, part 1

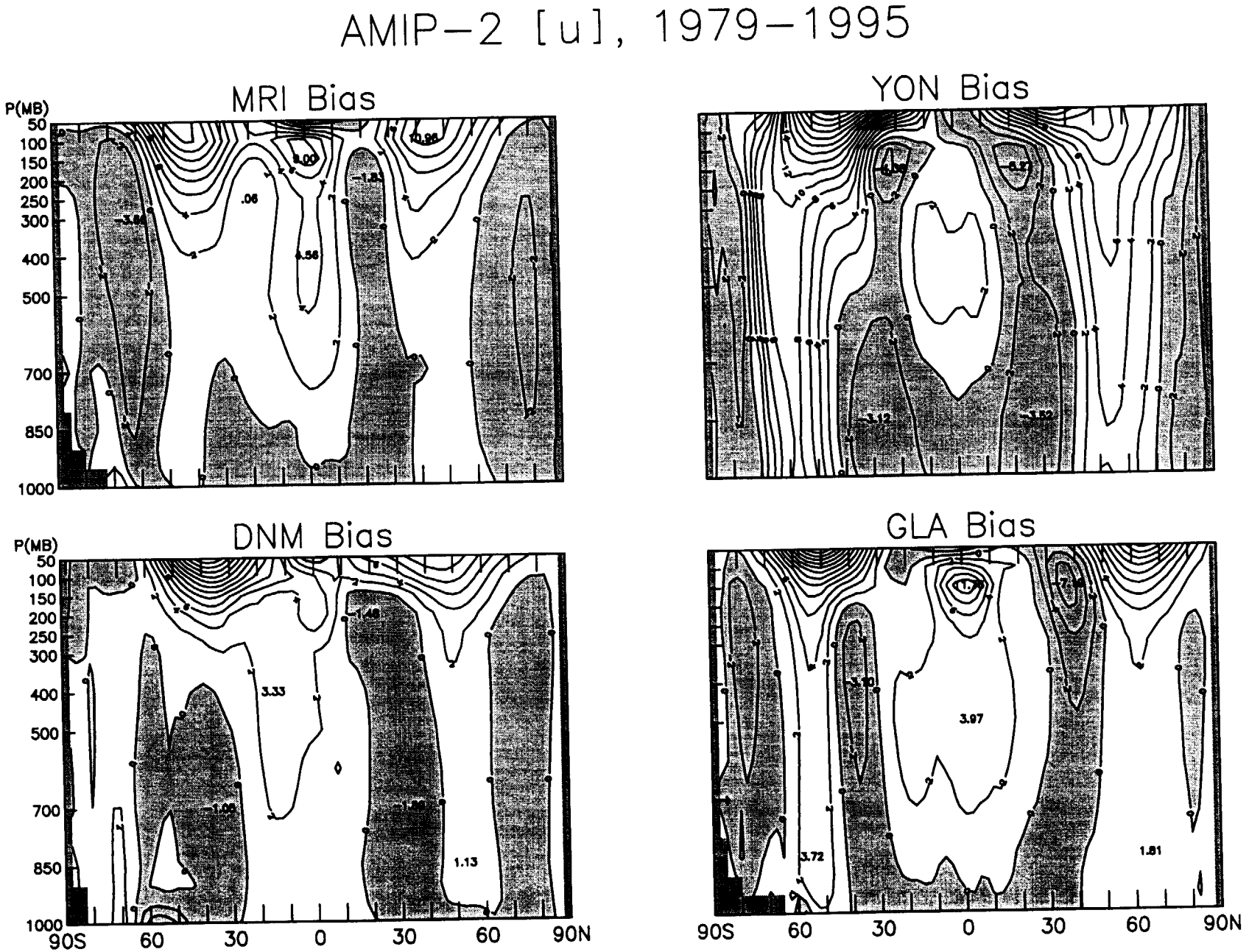
AMIP−2 [u], 1979−1995
MRI Bias
YON Bias
DNM Bias
GLA Bias
P(MB)
50
100
150
200
250
300
400
500
700
850
1000
90S
60
30
0
30
60
90N

Fig. 2.4, part 2

AMIP−2 [u], 1979−1995

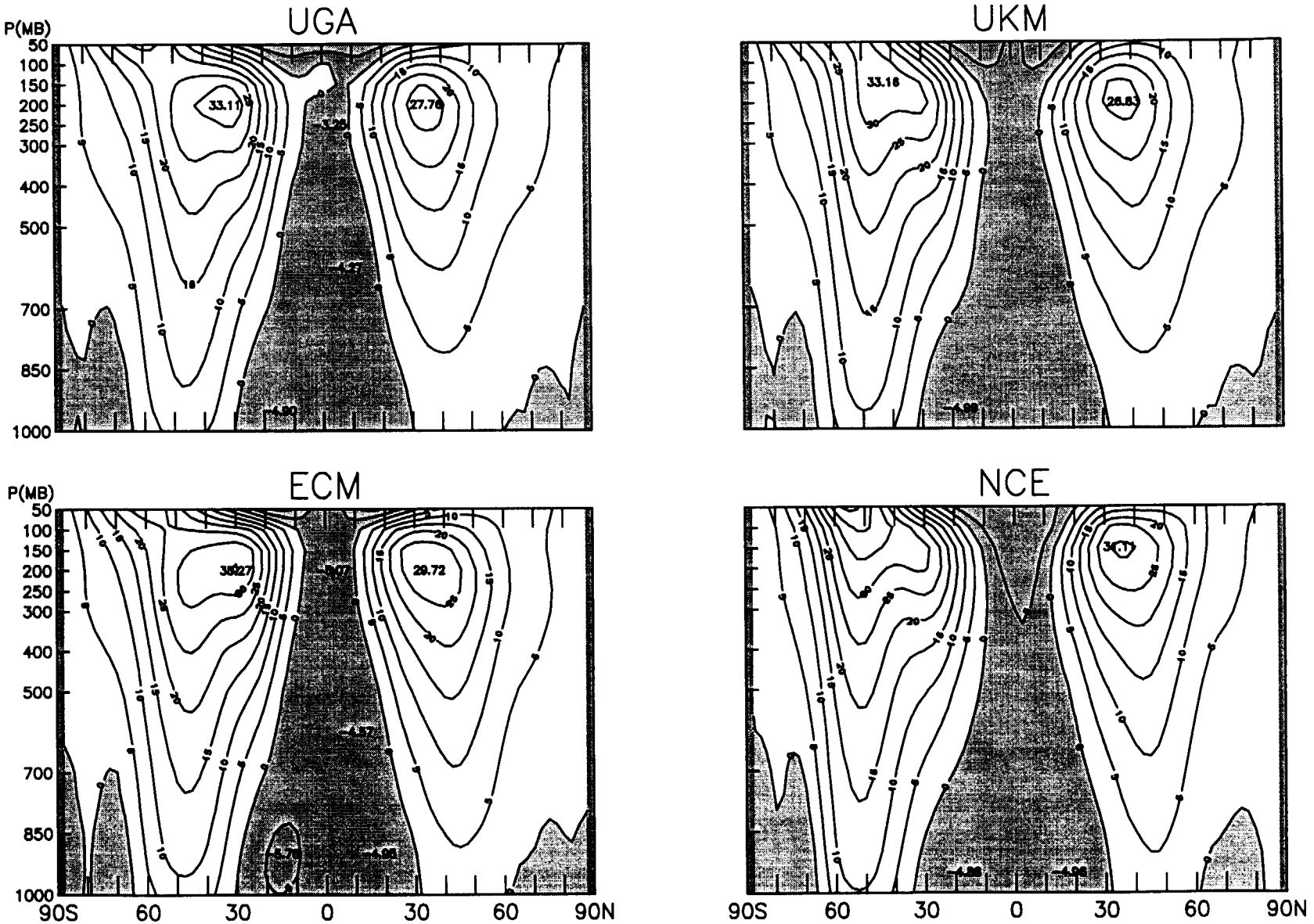

Fig. 2.5, part 1

AMIP–2 [u], 1979–1995

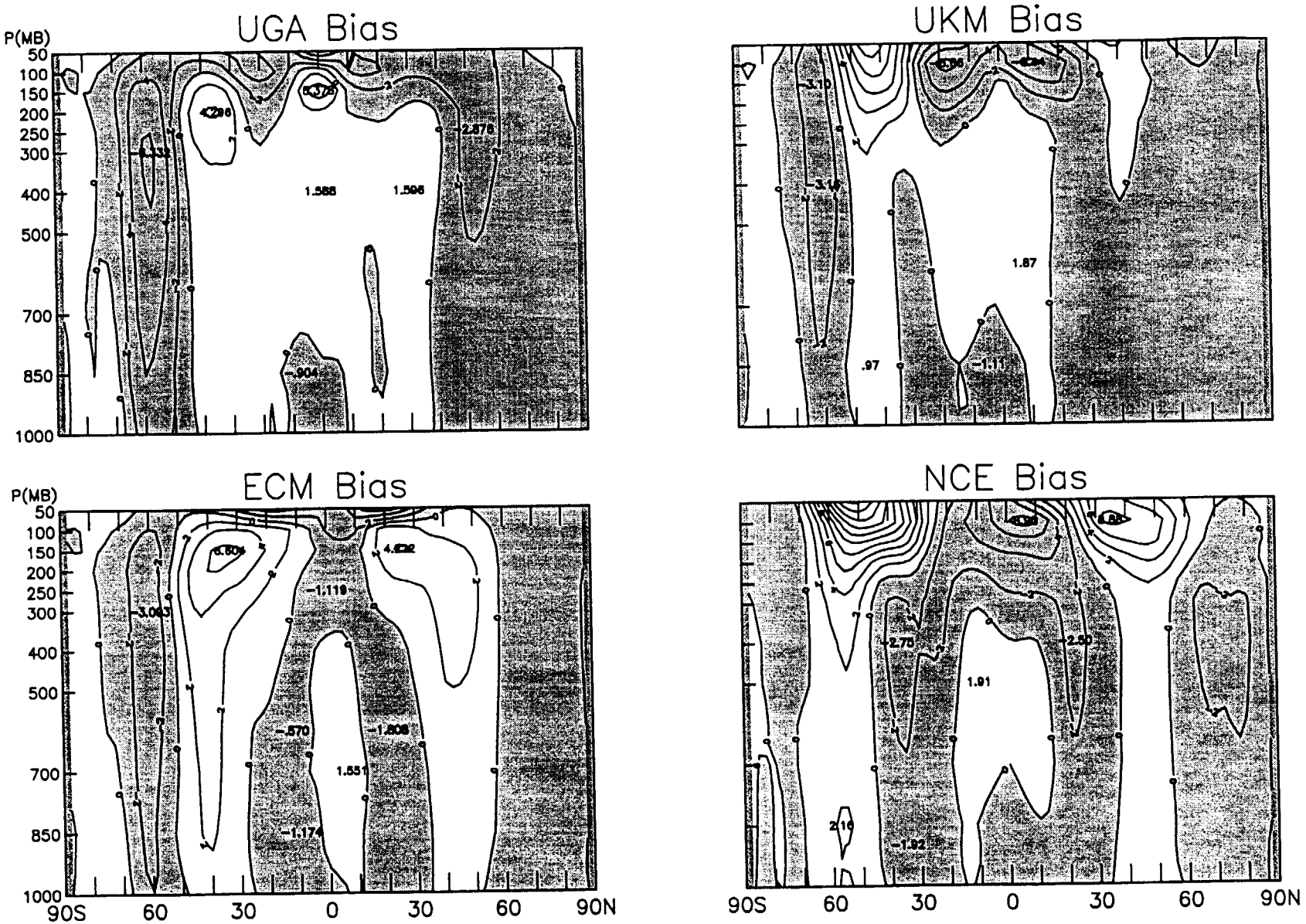

Fig. 2.5, part 2

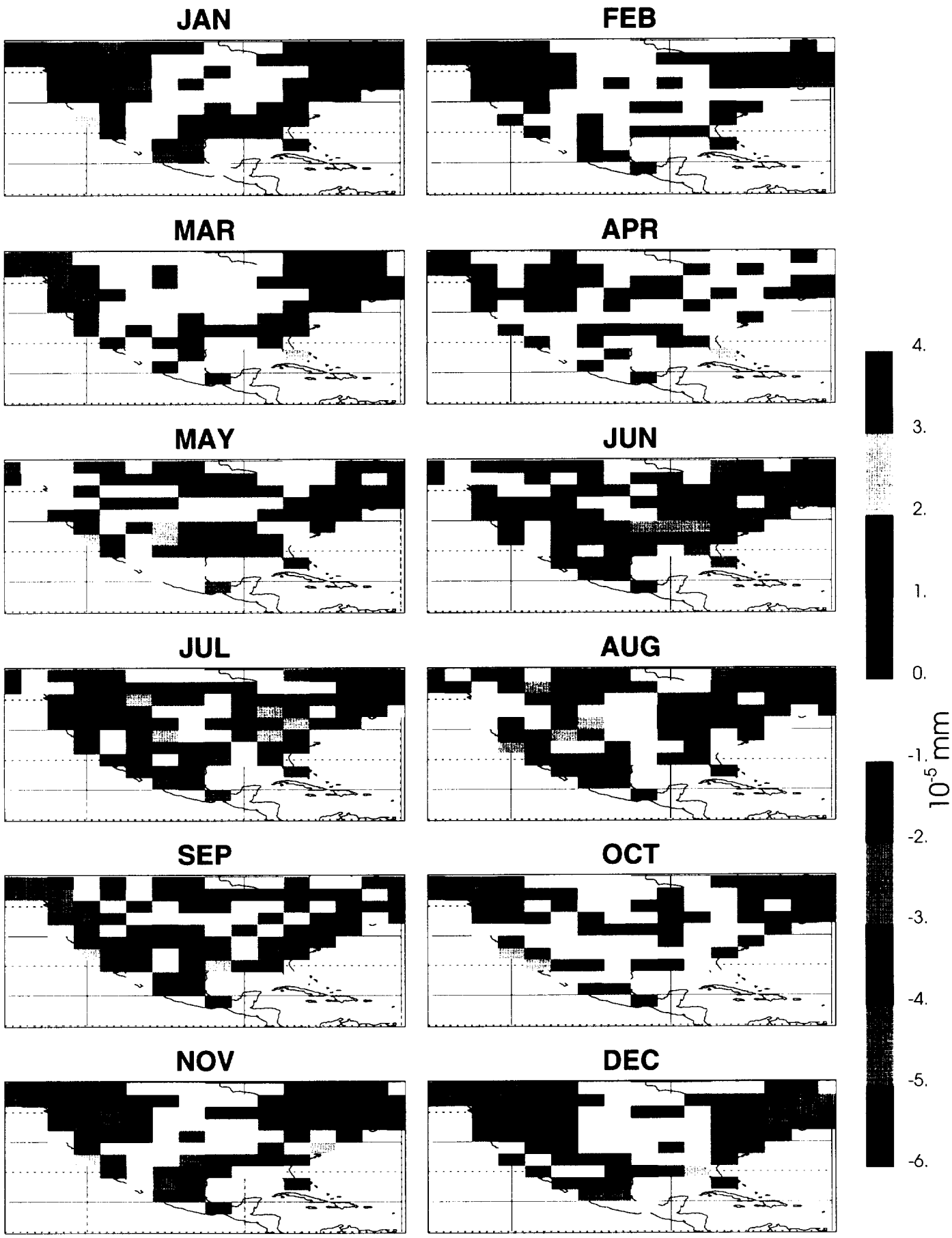
NASA Goddard MDL Mean div(Q) (1987-1990)
JAN
FEB
MAR
APR
MAY
JUN
JUL
AUG
SEP
OCT
NOV
DEC
4.
3.
2.
1.
0.
-1.
-2.
-3.
-4.
-5.
-6.
10-5 mm

Fig. 2.6

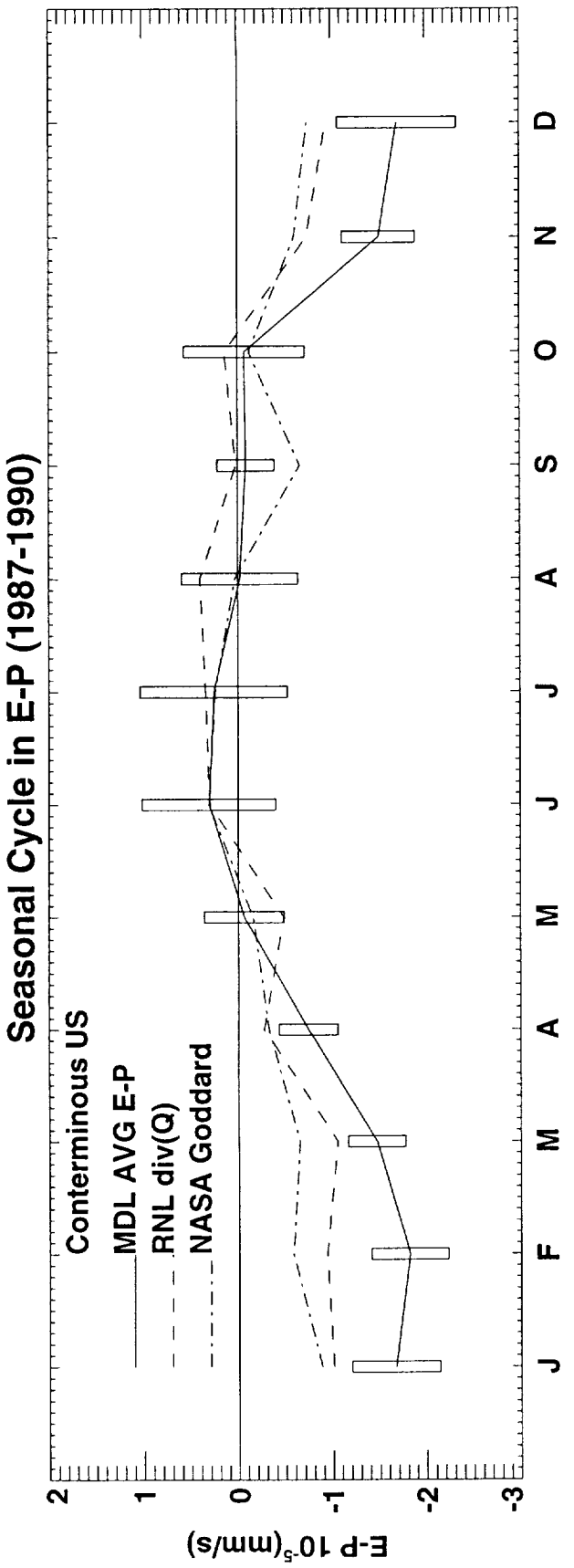
Seasonal Cycle in E-P (1987-1990)
Conterminous US
MDL AVG E-P
RNL div(Q)
NASA Goddard
E-P 10-5(mm/s)
2
1
0
-1
-2
-3
J
F
M
A
M
J
J
A
S
O
N
D

Fig. 2.7

Diabatic heating and the Atmospheric Energy Cycle

David A. Salstein
Atmospheric and Environmental Research, Inc., Cambridge, MA 02139, USA

1. Conservative quantities and their budgets

The overall energy of the atmosphere falls into the class of conservative quantities. As such, in the absence of exchanges of heat or other energy from outside the atmosphere, the total energy of the atmospheric system remains fixed, although it can change its form. Other examples of conservative properties in the atmosphere are angular momentum and mass, the latter counting dry air and of water mass separately; such a quantity cannot change its amount unless specific transfers occur from outside a system. This framework of conservative atmospheric processes was much appreciated and researched by Prof. Peixoto in a series of papers. His seminal book with Dr. A.H. Oort (Peixoto and Oort, 1992) was a culmination of much of that research.

Atmospheric angular momentum, for example, only changes by transfers across the surface below, but these can be important (e.g., Rosen, 1993). Thus, the changes in the angular momentum of the atmosphere are observed to cause very small but measurable variations in the rotation rate of the earth, as reckoned by changes in the length of day (Fig. 1). As a second example, the total water mass of the atmosphere is modified by exchanges of water substance into and out of the atmosphere, accomplished by means of precipitation and evaporation. Prof. J. P. Peixoto was the author of many papers concerning moisture fluxes and divergences (e.g. Peixoto, 1959; Starr et al., 1965). Such a divergence calculation using recent data over part of North America, a region that has long been the focus of intensive water resources studies, is given in Fig. 2.

2. Diabatic heating, total and components

Here we make a distinction of true heating, which changes the energy of a fluid, termed "diabatic," in contrast with those temperature tendencies of a fluid that are due merely to changes in pressure ("adiabatic"). Relevant processes that heat the atmosphere diabatically consist of sensible heating, by contact with either other air parcels or a surface, by latent heat release from phase changes of water vapor, by means of shortwave radiation from solar heating, and longwave radiational emission, a cooling (negative heating) process. The total diabatic heating is the sum of these individual processes. Because the diabatic heating components cannot be directly observed, we can turn to an atmospheric general circulation model to estimate them. The atmospheric model may be used alone, as a simulation, with only initial and boundary conditions; however, when it is part of a model-assimilation system it will make use of the observations as well to define the state of the atmosphere. Estimating rates of diabatic heating in such a way is, of course, greatly dependent upon the details and parameterizations of the particular model used.

An alternative to determining the total diabatic heating information is to examine the overall thermodynamic changes and infer the heating field that must cause such a change. This method will produce total diabatic heating, but not the individual components of diabatic heating. In comparing the sum of the diabatic components to the thermodynamics-derived fields, we can gain confidence in the models used. In fact, the best success in this comparison is at the lowest levels. The principal advantage to the component method is that by using it we can understand how each physical mechanism

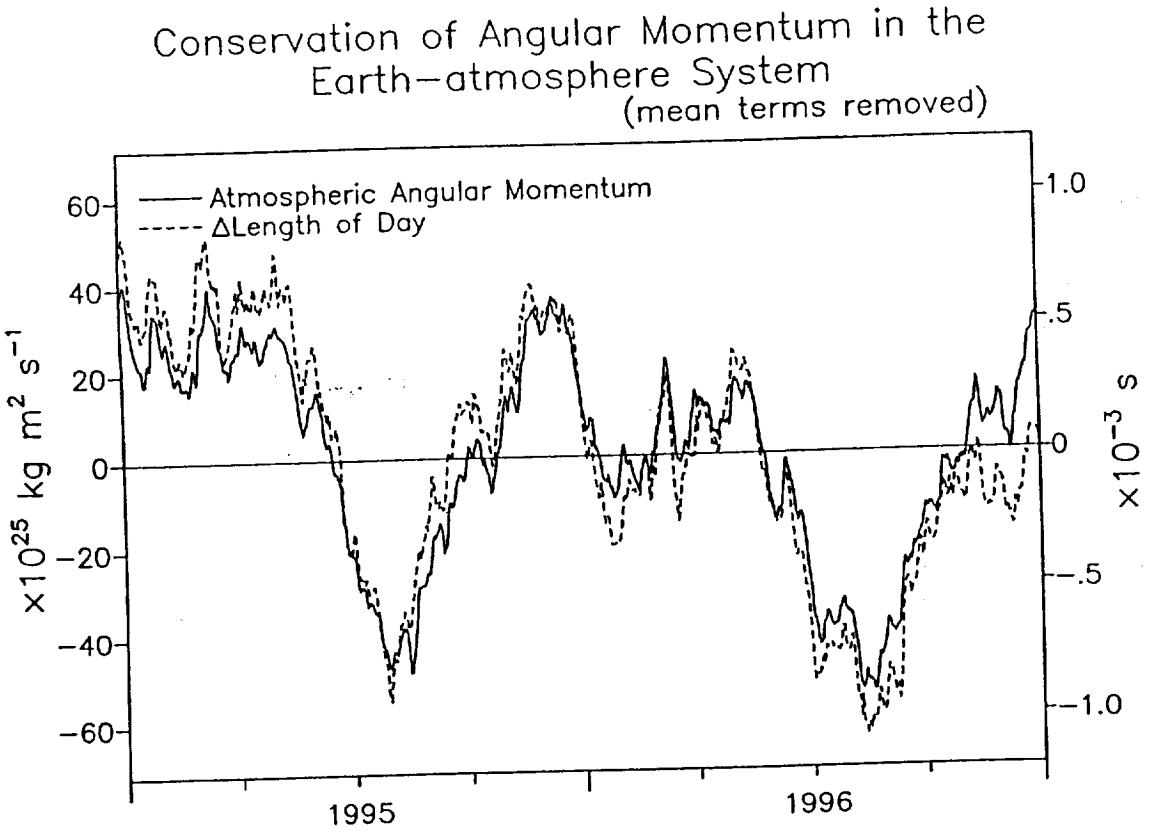

Fig. 1. The angular momentum of the atmosphere based on zonal winds from the NCEP/NCAR reanalysis system (solid line, scale at left) for a two-year period, and departures of the length of day from a constant (dashed line, scale on right). Mean terms are removed. Conservation of angular momentum would imply a near agreement on the scales plotted.

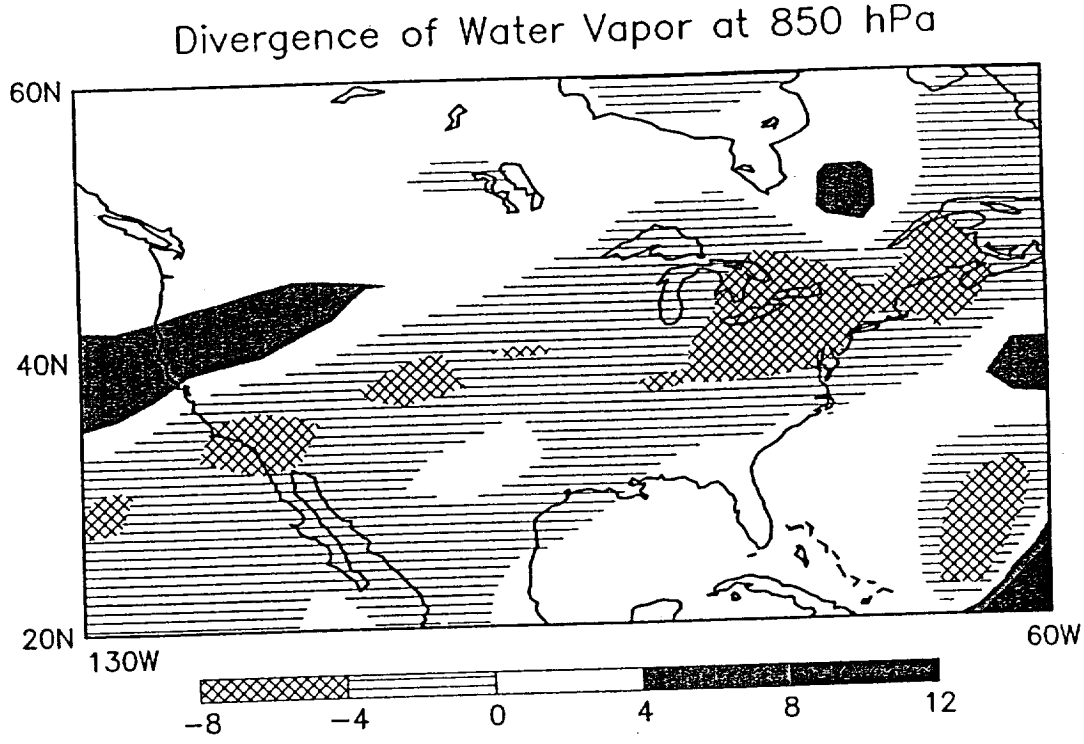

Fig. 2. Divergence of water vapor at 850 hPa based on the NCEP/NCAR reanalysis system. Vertical integrals of this term may be matched to the difference between evaporation and precipitation to the estimated conservation of water mass based on the models.

contributes to the energy cycle independently, through the generation of available potential energy.

We first determined the diabatic heating components with the United States' National Aeronautics and Space Administration (NASA)'s Goddard Laboratory for Atmospheres analyses for some months of the Global Weather Experiment (GWE) in 1978-1979. Subsequently we have examined the diabatic heating rates and energy cycle from 14 years of output from a later period, the full calendar years of 1981-1994. This period was part of the continuation from the GWE, and uses the Goddard Earth Observing System Data Assimilation System, on which we will concentrate here (Schubert et al., 1983).

We note that the largest portion of the latent processes results from condensation due to the process of cloud formation. It may occur by means of a number of distinct subprocesses, including those on large scales and those on the smaller convective scales. Conversely, latent processes also cool the atmosphere as a result of evaporation, principally near the ground.

Sensible heating involves contact with the ground, as well as transfer of heat between levels within the atmosphere. Much of the transport from the ground takes place by means of turbulent exchanges in the boundary layer, also considered one of the sensible heating processes. Above the boundary layer, sensible heating exchanges are considerably weaker.

Shortwave radiation from the sun peaks in the visible band, near wavelength 0.5 μm, whereas longwave processes, that is to say, radiational emission from the Earth, peak in the infrared near 10 μm. This difference between the maximum frequency for solar and terrestrial radiation is a result of Wien's law, which states that the wavelength of maximum emission is inversely proportional to the temperature of the emitting body. The principal gases that absorb solar radiation include water vapor molecules of the lower atmosphere and carbon dioxide. The strength of the input solar radiation varies strongly with time of day and season, due to the variability in the angle at which the radiation passes through the atmosphere.

3. Diabatic heating components from runs of the Goddard data assimilation system

Taken from the long-term simulations of the NASA Goddard Laboratory for Atmospheres Data Assimilation System, the diabatic heating components are quite dependent on both latitude and height, as shown by the zonal mean heating in Fig. 3.

Longwave radiational processes produce negative heating everywhere but the strongest areas of this cooling are found just above the earth's surface, in the lower latitude subtropics. Shortwave heating is positive, with strongest values near the lower latitudes and in the lower troposphere. Sensible heating is concentrated near the ground, and reaches a mean rate of nearly 3 K day^{-1}. The value of latent heating has its largest maximum in the tropics near the 500 mb level (also 3 K day^{-1}) due to strong convection there. Secondary maxima occur in the middle to higher latitudes.

A summary of the heating processes may be reviewed by examining maps at each pressure level. For example, sensible heating during January 1986 at the 950-hPa level (Fig. 4) is strong over the Southern Hemisphere continents, where the summer land surface is warm and over the relatively warm currents in the North Atlantic and North Pacific Oceans (the Gulf Stream and the Kuroshio, respectively).

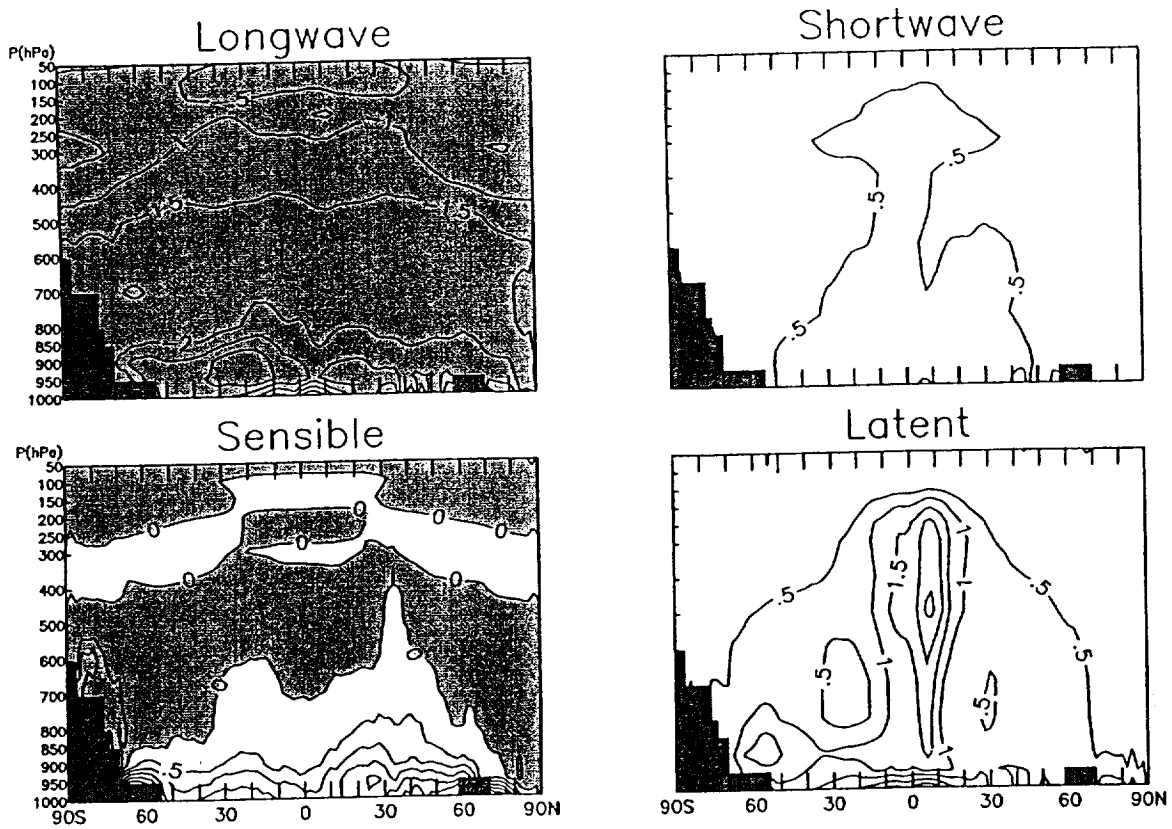

Fig. 3. Zonal mean values of the four forms of diabatic heating for the mean period 1981-1994, based on the NASA GEOS-1 Data Assimilation System. Units are K day^{-1}.

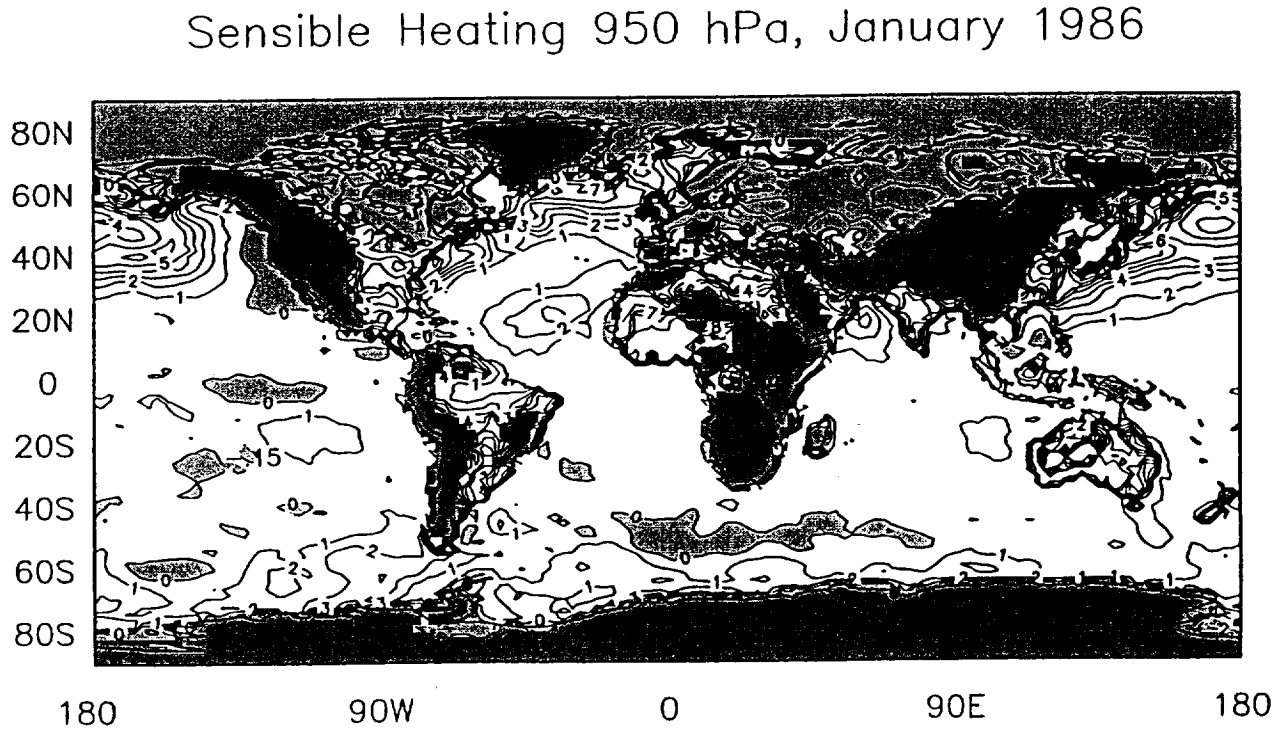

Fig. 4. Mean sensible heating for January 1986 at the 950-hPa level from the NASA GEOS-1 Data Assimilation System. Units are K day^{-1}.

The latent processes within the model, in particular, are sophisticated, and involve complex motions with cloud convection schemes (Arakawa and Schubert, 1974; Sud and Walker, 1993). At higher levels, near 400-500 hPa, very deep convection produces strong latent heating over areas including the western tropical Pacific and maritime continent (Indonesia), across to India, and over much of the areas close to the equator. Minima in latent heating occur in the sub-tropics, in the region of reduced convection near the descending portions of the mean meridional circulation cells, like the Hadley circulation. Further poleward, maxima in the latent heating rates occur again, with the middle latitude values resulting from shallower convective activity and large-scale cloudiness, though some deeper convection can occur there too.

The zonal and vertical mean heating can be understood in the synthesis in Fig. 5 in which a meridional profile of all four terms and the total are given. In this case (for a January period), the latent heating is clearly strongest, and essentially, contains the shape of the total, whereas the longwave process provides negative heating throughout. Indeed, the longwave, shortwave and sensible processes appear very nearly to cancel, providing reconfirmation of the importance of the latent heating.

Interestingly, keeping track of the diabatic heating, particularly the sensible heating throughout the diurnal cycle is important too. The strong value of sensible heating occurs around local noon over the continents (e.g., for the southern hemisphere, Australia at 6 UT, Africa at 12 UT, and South America at 18 UT). It is important thus to maintain the records several times per day to get a complete picture of the heating and energy balance of the atmosphere.

4. Generation of available potential energy

Although diabatic heating yields energy input into the whole system, how the heating is distributed within the system is important to whether it can be transformed to other forms of energy. If the diabatic heating distribution is applied uniformly, it will tend to raise the temperature of a large area evenly. Although the total energy of the system would be modified in this case, in the form of internal energy, this additional energy cannot be released into the kinetic energy form, which requires heating by uneven horizontal gradients to increase the "available potential energy (APE)" of the system. The APE relates to the differences in temperature (density) of air particles all located at the same geopotential level. When such differences in temperature gradient exist, the atmosphere can potentially rearrange its state by air movements to eliminate such a gradient; in this case the available potential energy would be converted into kinetic energy, and, in so doing, tend to eliminate the temperature gradient on the same equipotential.

For APE to increase requires the distribution of diabatic heating to be positively correlated with the temperature field on a given equipotential surface. In that case, the areas that start warmer than the spatial temperature mean will become relatively warmer yet, while the colder areas will increase their relative negative temperature anomaly because of a heating deficit. Thus, the combined spatial distribution of heating and temperature is instrumental to the generation of APE from diabatic heating.

As described above, the values of the sensible, latent, and shortwave radiational heating components all generally decrease from equator to poles, and they are thus positively correlated with the mean temperature pattern. Because of this distribution, their actions lead to act to increase the existing meridional temperature gradient, and in so doing have the capacity to increase the potential energy available for the atmosphere to convert to kinetic energy. Conversely, longwave radiation is negatively correlated with

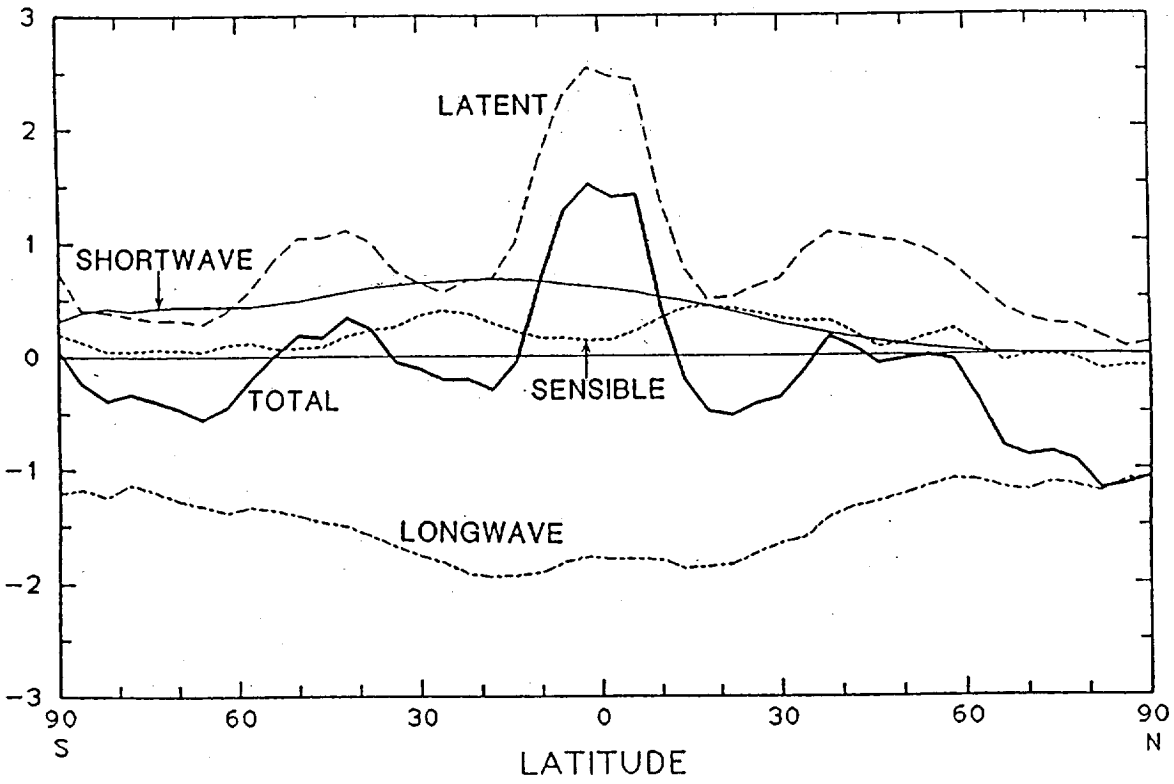

Fig. 5. The vertical mean components of diabatic heating and total heating for a January month, based on the NASA Goddard Data Assimilation System. Units are K day^{-1}.

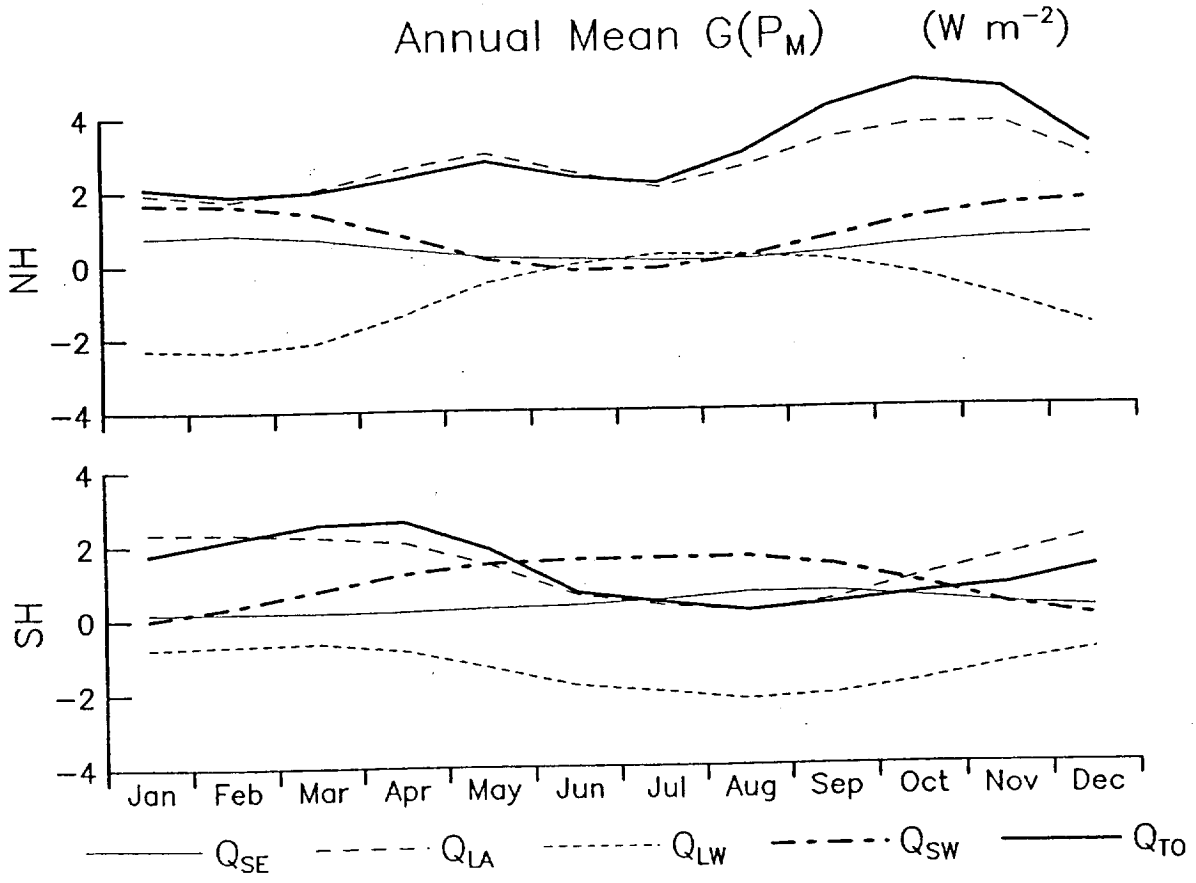

Fig. 6. Mean annual signal for the generation of zonal mean available potential energy between 1980 and 1995 from each of the diabatic heating (Q) components. Here SE=sensible; LA=latent; LW=longwave; SW=shortwave; TO=total). Units are W m^{-2}.

temperature, cooling in relatively warm areas, and vice versa. Longwave radiation thus acts to reduce this potential energy. Nevertheless, the reduction due to the longwave term is less than those of the other three diabatic heating terms, and so, overall, the meridional distribution of heating helps to maintain the energy cycle of the atmosphere's general circulation.

Available potential energy can be generated by the zonal mean state, or it can be generated by the action of eddies, either transient or standing. To calculate the generation of zonal mean APE requires the use the anomalous temperature and heating fields. From an analysis of the generation of APE between 1980 and 1995 with the NASA Goddard data assimilation system, the effect of sensible, shortwave and longwave tend to cancel, while the generation G(APE) due to latent heating is rather close to that of the total. There are anomalies at the months around the El Niño/La Niña cycles in 1982-1984 and 1986-1987. The annual mean values for G(APE) from the four processes for the two hemispheres is given in Fig. 6 and also shows how the total signal is similar to the latent contribution alone.

5. Role of the generation of available potential energy in the energy cycle

The energy of the atmosphere can be viewed as generated to be available potential energy from the diabatic heating fields, in either mean or eddy forms, and converted to kinetic energy by the act of eddies or by mean atmospheric overturning. A view of these processes is given in the energetics flowchart in Fig. 7 (top). Given a computer simulation of the atmosphere using the data assimilation system of the NOAA Geophysical Fluid Dynamics Laboratory, we can determine many of these energetics numbers and we show them in Fig. 7 (bottom). We also determine, by residual means in the sense of Fig. 7b, the generation of available potential energy for this period in both the zonal mean and eddy forms (bottom lines in both parts of Table 1). The top sets in Table 1 show the generation of available potential energy from each of the components of diabatic heating, from the NASA Goddard Laboratory for Atmospheres system. The zonal mean values, $G(P_M)$, are stronger than the eddy values, $G(P_E)$, but, again, the latent heating component is the largest in both forms.

The sum of the contributions from all four components can be compared with the values from residual method. Given the uncertainties in all these numbers and the fact that the total diabatic involves values of both signs, the two methods produce relatively close values. It is still uncertain, however, which technique of the two is better to use to determine values for the generation of available potential energy.

6. Summary

Energy, like angular momentum and mass, is a property of the atmospheric system subject to conservation, which was a fundamental view in Prof. Peixoto's work. In this light, we turned to estimates of the diabatic heating of the atmosphere to understand how the energy from this heating is distributed throughout the atmosphere and drives the atmospheric energy cycle through the generation of available potential energy.

However, the components of diabatic heating can only be determined with the aid of a modern analysis-forecast system, and to do so adequately requires calculations several times per day. By looking at the diabatic heating in this way, we can also examine the generation of APE in zonal mean and eddy forms, and we are led to an understanding of how the different processes are responsible for driving the general circulation. Latent heating has a particularly strong role in the generation of available potential energy.

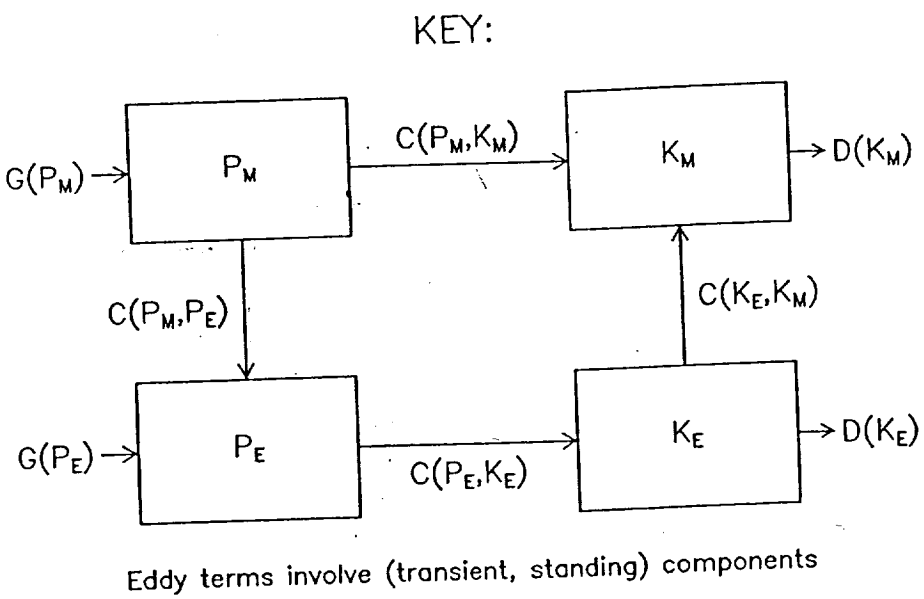

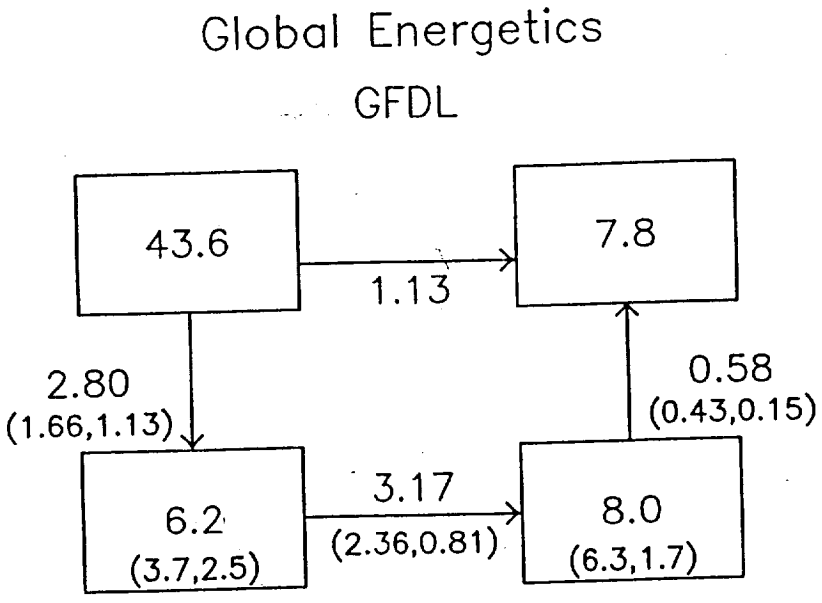

Fig. 7. (a) Key for the energy cycle involving available potential energy (P) and kinetic energy (K) terms). Subscripts M and E indicate zonal mean and eddy forms. Conversions (C terms;) are from the first quantity to the second quantity written in parentheses. G and D indicate generation and dissipation terms respectively. (b) Values for the energy (units 10^5 J m^{-2}) and conversion (units W m^{-2}) terms in the energy cycle for the globe, according to the key in (a), from the NOAA Geophysical Fluid Dynamics Data Assimilation System.

Acknowledgments. The author wishes to acknowledge the kindness and hospitality of his Portuguese hosts during the symposium. The United States National Aeronautics and Space Administration (NASA) supported the research through contract NAS5-98179.

References

Arakawa, A., and W. H. Schubert, 1974: Interaction of cumulus cloud ensemble with the large-scale environment, Part I. *J. Atmos. Sci.*, 31, 674-701.

Oort, A.H., 1974: On estimates of the atmospheric energy cycle, *Mon. Wea. Rev.*, 11, 483-493.

Peixoto, 1959; O campo da divergência do transporte do vapor da agua na atmosfera. *Revista da Faculdade de Ciências de Lisboa*, 2A, Ser. B, Vol. VilI, pp. 25-56.

Peixoto, J.P. and A.H. Oort, 1992: *Physics of Climate*, AIP Press, 520 pp.

Rosen, R.D., 1993: The axial momentum balance of Earth and its fluid envelope. *Surveys in Geophysics, 14,* 1-29.

Schubert, S., R. Rood, and J. Pfaendtner, 1993: An assimilated data set for Earth science applications, *Bull. Am. Meteorol. Soc.*, 74, 2331-2342.

Starr, V.P., and J.P. Peixoto, 1965: The hemispheric eddy flux of water vapor and its implications for the mechanics of the general circulation. *Archiv. Fur Meteorologie, Geophysick und Bioklimatologie.*

Sud, Y.C. and G.H. Walker, 1993: A rain evaporation and downdraft parameterization to complement a cumulus updraft scheme and its evaluation using GATE data. *Mon. Wea. Rev.*, 121, 3019-3039.

$G(P_M)$

Shortwave	1.66
Longwave	-3.05
Sensible	0.49
Latent	3.72
Total diabatic	2.82
Residual method /GFDL	*(3.92)*

$G(P_E)$

Shortwave	0.11
Longwave	-0.31
Sensible	-0.07
Latent	0.56
Total diabatic	0.29
Residual method /GFDL	*(0.37)*

Table 1. The generation of zonal mean (M) and eddy (E) available potential energy over the globe from each of four heating components and the total diabatic heating for an annual period, based on the NASA GEOS-1 Data Assimilation System. The lowest line of each part indicates the generation terms based on a residual method (using the GFDL system) for a similar period. Units are W m^{-2}.

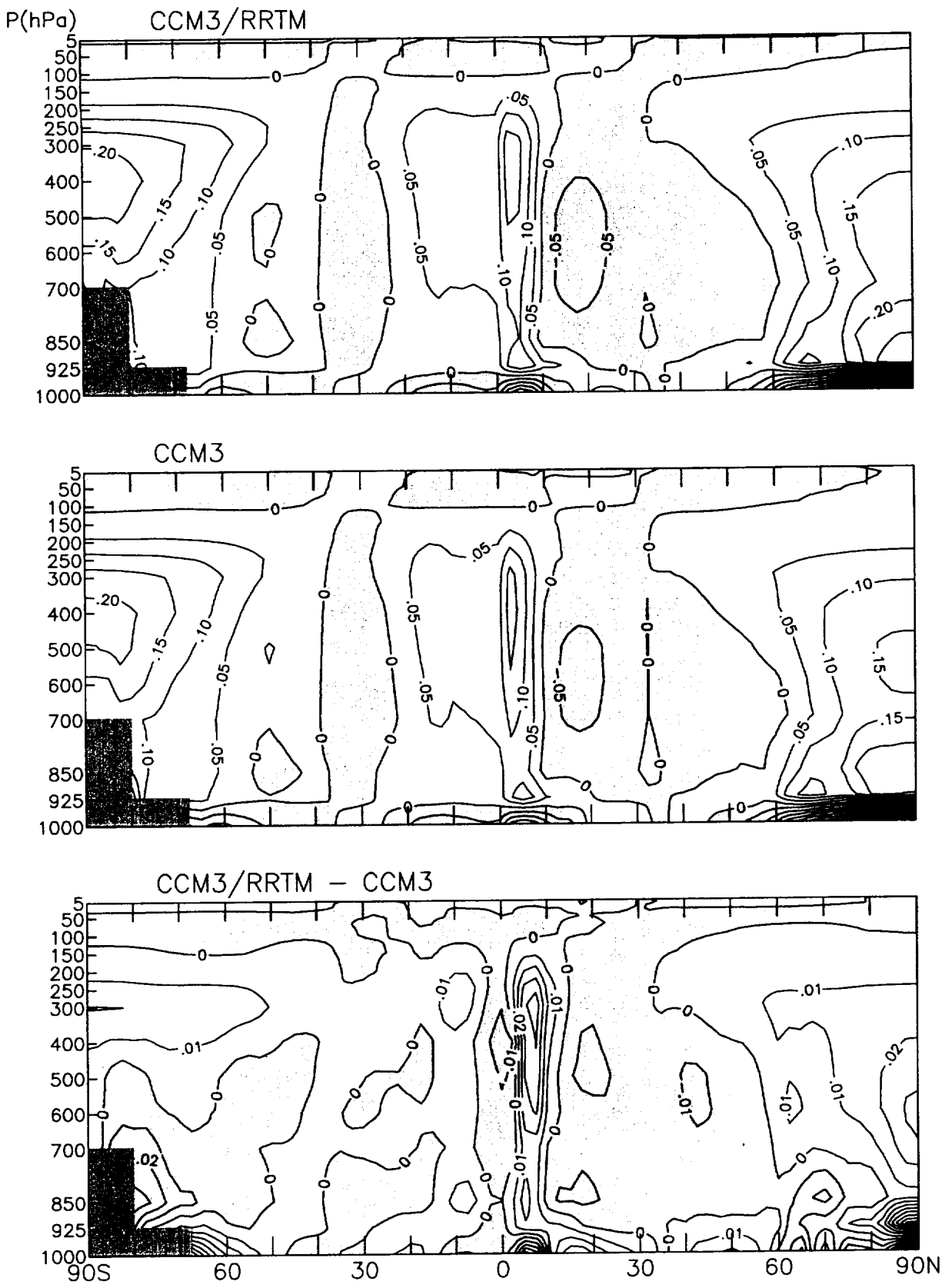
Generation of APE (by Latent), Mean Jan. (W kg^{-1})
P(hPa)
CCM3/RRTM
CCM3
CCM3/RRTM – CCM3
5
50
100
150
200
250
300
400
500
600
700
850
925
1000
90S
60
30
0
30
60
90N

Fig. 3a.1

Attachment 4 – Manuscript submitted to a journal; title and abstract below.

A dynamical framework to understand and predict the major Northern Hemisphere climate mode

Judah Cohen, David Salstein and Kazuyuki Saito

The dynamics of the leading mode of boreal winter and its excitation by varying boundary conditions remain mostly unclear. A novel framework is presented to explain the evolution of this dominant winter mode. It is shown that there exists a dichotomy of pathways with the characteristics of the dominant mode dependent upon the pathway taken. All winters examined fall into one of the two different dynamic evolutions presented, the knowledge of which clarifies prior uncertainties associated with the dominant mode and provides excellent potential for the successful prediction of subsequent winter mean climate states.

REPORT DOCUMENTATION PAGE

Form Approved
OMB No. 0704-0188

1. AGENCY USE ONLY *(Leave blank)*	2. REPORT DATE 1 September 2001	3. REPORT TYPE AND DATES COVERED Annual, Option 1

4. TITLE
Momentum and energy assessments with NASA and other model and data assimilation systems

5. FUNDING NUMBERS
NAS5-98179

6. AUTHORS
David Salstein, Peter Nelson, Wenjie Hu

7. PERFORMING ORGANIZATION NAME(S) AND ADDRESS(ES)

Atmospheric and Environmental Research, Inc.
131 Hartwell Avenue
Lexington, MA 02421

8. PERFORMING ORGANIZATION REPORT NUMBER
P785

9. SPONSORING/MONITORING AGENCY NAME(S) AND ADDRESS(ES)

National Aeronautics and Space Administration
Goddard Space Flight Center
Greenbelt, MD 20771

10. SPONSORING/MONITORING AGENCY REPORT NUMBER

11. SUPPLEMENTARY NOTES

12a. DISTRIBUTION/AVAILABILITY STATEMENT

12b. DISTRIBUTION CODE

13. ABSTRACT *(Maximum 200 words)*

14. SUBJECT TERMS

15. NUMBER OF PAGES
33

16. PRICE CODE

17. SECURITY CLASSIFICATION OF REPORT	18. SECURITY CLASSIFICATION OF THIS PAGE	19. SECURITY CLASSIFICATION OF ABSTRACT	20. LIMITATION OF ABSTRACT
Unclassified	Unclassified	Unclassified	Unlimited